ACS OMEGA

Open Access

http://pubs.acs.org/journal/acsodf

Article

Accumulation and Quantitative Assessment of Terrigenous Organic Matter in Upper Oligocene to Lower Miocene Marine Source Rocks of the Qiongdongnan Basin

Ziming Zhang, Dujie Hou,* Changgui Xu, Keqiang Wu, Li You, Xiong Cheng, Xiaze Yan, and Weihe Chen

Cite This: *ACS Omega* 2024, 9, 22903−22922

Read Online

ACCESS | Metrics & More | Article Recommendations | Supporting Information

ABSTRACT: The intense collision between marine and terrestrial agents results in the dual-source (marine and terrigenous) characteristics of marine source rocks. Our research quantitatively assessed terrestrial organic matter and revealed the crucial role of terrestrial organic materials in the organic matter enrichment of lower Miocene to upper Oligocene marine source rocks in the Qiongdognnan Basin. The quantitative assessment was achieved using partial least-squares analysis with eight biomarker parameters associated with *n*-alkanes, isoprenoids, bicadinanes, taraxerane, tricyclic terpanes, and gammacerane. Differential unloading of terrestrial organic materials based on sedimentary facies of the delta-marginal sea system were observed through oleanane and bicadinane contents. It should be noted that the diagnostic ratio of oleanane was excluded from the quantitative analysis due to the dual influence from differential unloading and contact with seawater of the terrestrial organic materials. Calculation results show that the terrestrial organic matter was highest in the delta front at 70%, followed by prodelta at 59% and inner shallow marine at 57%. From the late Oligocene to the early Miocene, the proportion of terrestrial organic matter in marine source rocks continuously increased, with the highest average value observed in the second member of the Sanya Formation at 69% and the lowest occurring in the third member of the Lingshui Formation at 46%. Increasing terrestrial organic material inputs and preservation driven by the East Asian summer monsoon provided first-order control of the accumulation of organic carbon in the Qiongdongnan Basin during late Oligocene to early Miocene, rather than the bioproductivity of marine algae. The redox conditions of the water column determine the enrichment extent of organic matter.

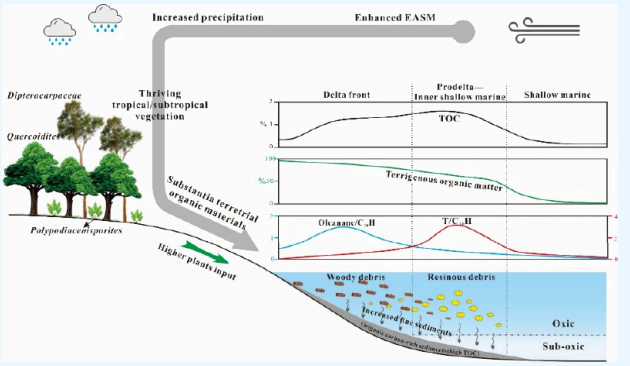

1. INTRODUCTION

The delta plays an important role in Source-to-Sink in the Qiongdongnan Basin, as the intensive interactions between marine and terrestrial geological agents in delta-marginal sea systems result in a mixed geochemical characteristic of marine and terrestrial organic matter in marine source rocks.[1−4] Terrigenous organic matter preserved in marine sediment acts as a valuable recorder of paleovegetation and paleoclimatic variations in the source areas.[5] Tracing their fates in delta-marginal sea systems can help understanding the enrichment mechanisms of organic matter in marine source rocks.[1,6] The occurrence of high contents of oleanane-type terpanes and bicadinanes in the Qiongdongnan Basin confirmed the angiosperm sources.[7] However, multiphased tectonic activities, variable depositional environments, and transitions in paleoclimates disturbed the distribution of terrigenous organic matter in the Qiongdongnan Basin.[3,8] Previous scholars mainly focused on the molecular geochemical characteristics and paleovegetation reconstruction in the Qiongdongnan Basin, giving little attention to the quantitative evaluation of terrigenous organic matter in the marine source rocks.[5,7] The determination of the terrigenous organic matter proportion can provide deeper insights into migration patterns of terrestrial organic materials and track the fate of organic carbon in delta-marginal sea systems, making it worthwhile to pay more attention.[9−11] The proportion of terrestrial organic matter can be evaluated through carbon, hydrogen, and nitrogen isotopes, as well as the C/N ratio and sporopollen.[12−17] However, the application of these approaches is quite limited in petroleum exploration due to the complexity of the measurements. Our research quantified terrigenous organic matter using biomarkers for the first time,

Received: February 28, 2024
Revised: April 27, 2024
Accepted: May 7, 2024
Published: May 16, 2024

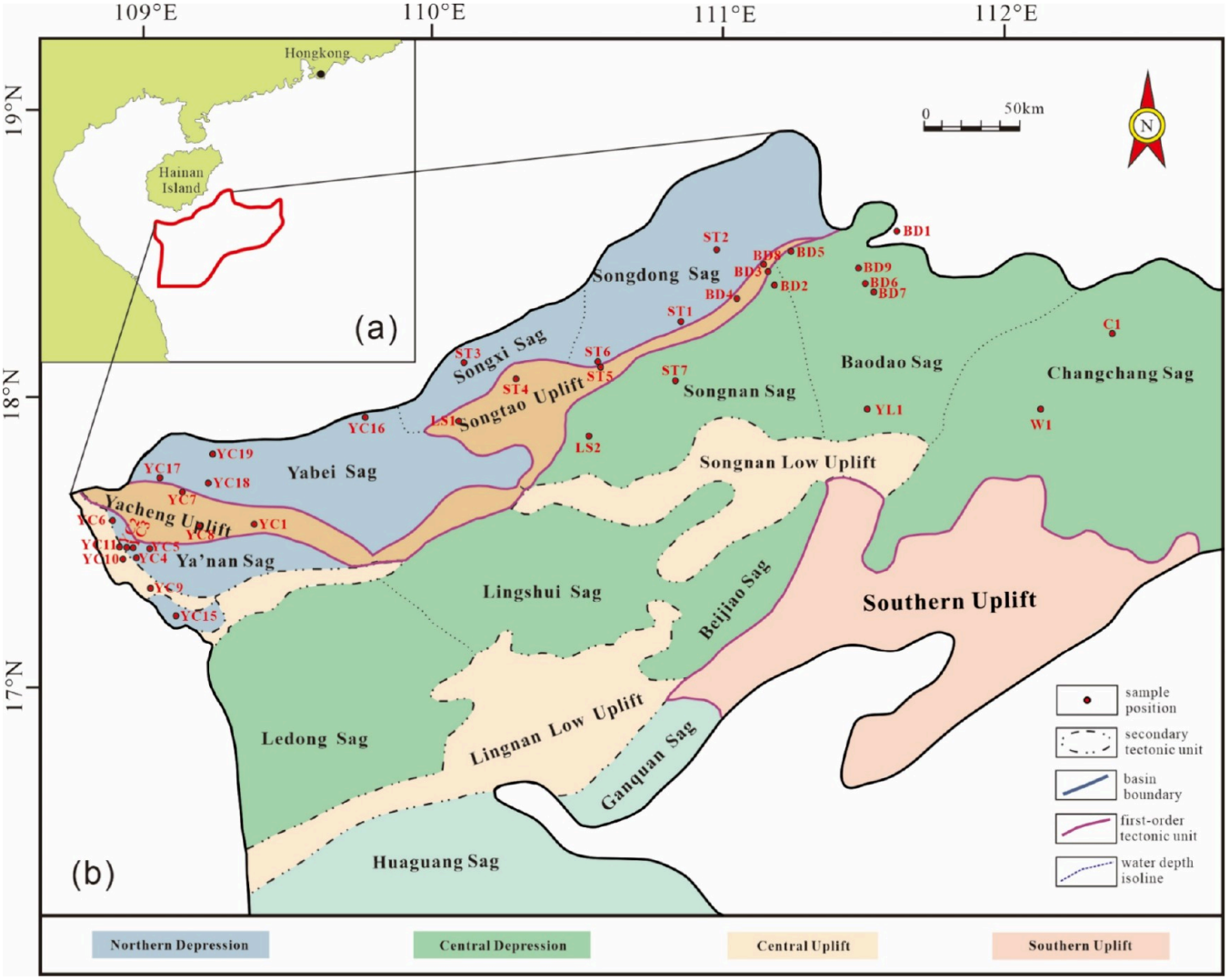

Figure 1. (a) Geological location and (b) subdivision of tectonic units of the Qiongdongnan Basin modified after Xu.[7] The critical wells are marked with red circles.

providing new insights into the controlling factors of organic carbon enrichment in the Qiongdongnan Basin.

In this study, systematic organic geochemical analyses were conducted on marine source rocks from the late Oligocene to early Miocene in the Qiongdongnan Basin. We screened eight saturated hydrocarbon biomarker parameters and attempted to establish a quantitative assessment method for terrigenous organic matter in marine source rocks. Based on the calculation results, the spatiotemporal signatures of terrigenous organic matter were quantitatively characterized. Finally, we advanced a new terrigenous organic matter enrichment model in the Qiongdongnan Basin.

2. REGIONAL SETTING

The Qiongdongnan Basin is an extensional sedimentary basin developed on the background of a Cenozoic fault depression and quasi-passive continental margin in the northern of the South China Sea with an area of about 80 000 km^2.[8] It can be divided into the Northern Depression, Central Depression, and Southern Depression based on the tectonic framework (Figure 1b). The Northern Depression includes the Songdong, Songxi, Yabei, and Ya'nan Sags, while the Central Depression contains the Changchang, Baodao, Songnan, Lingshui, and Ledong Sags. Due to the rapid deposition rate, the Cenozoic sediments in the basin exceed 12 000 m, including the Lingtou (T100−T80), Yacheng (T80−T70), Lingshui (T70−T60), Sanya (T60−T50), Meishan (T50−T40), Huangliu (T40−T30), Yinggehai (T30−T20), and Ledong (T20−) Formations from bottom to top.[18,19]

The Qiongdongnan Basin underwent a transgression process from the late Oligocene to the middle Miocene, with the sedimentary facies predominantly characterized as deltaic, littoral, shallow marine, and bathyal.[3] Three types of source rocks were determined in the past, including the Eocene lacustrine, the Oligocene marine-continental transitional coal measure, and the Oligocene to Miocene marine source rocks.[7,18,19] It should be noted that the Oligocene to Miocene marine source rocks in this study include marine terrigenous shales (deposited in the delta front and prodelta, marine−terrestrial transitional setting) and marine shales (deposited in the shallow marine, marine setting). They have received increasing attention in deep-water petroleum exploration.[2,4]

Our target strata (red rectangle in Figure 2) in this study are composed of the second member of the Sanya Formation (N_1s_2), the first member of the Lingshui Formation (E_3l_1), the

https://doi.org/10.1021/acsomega.4c01777
ACS Omega 2024, 9, 22903−22922

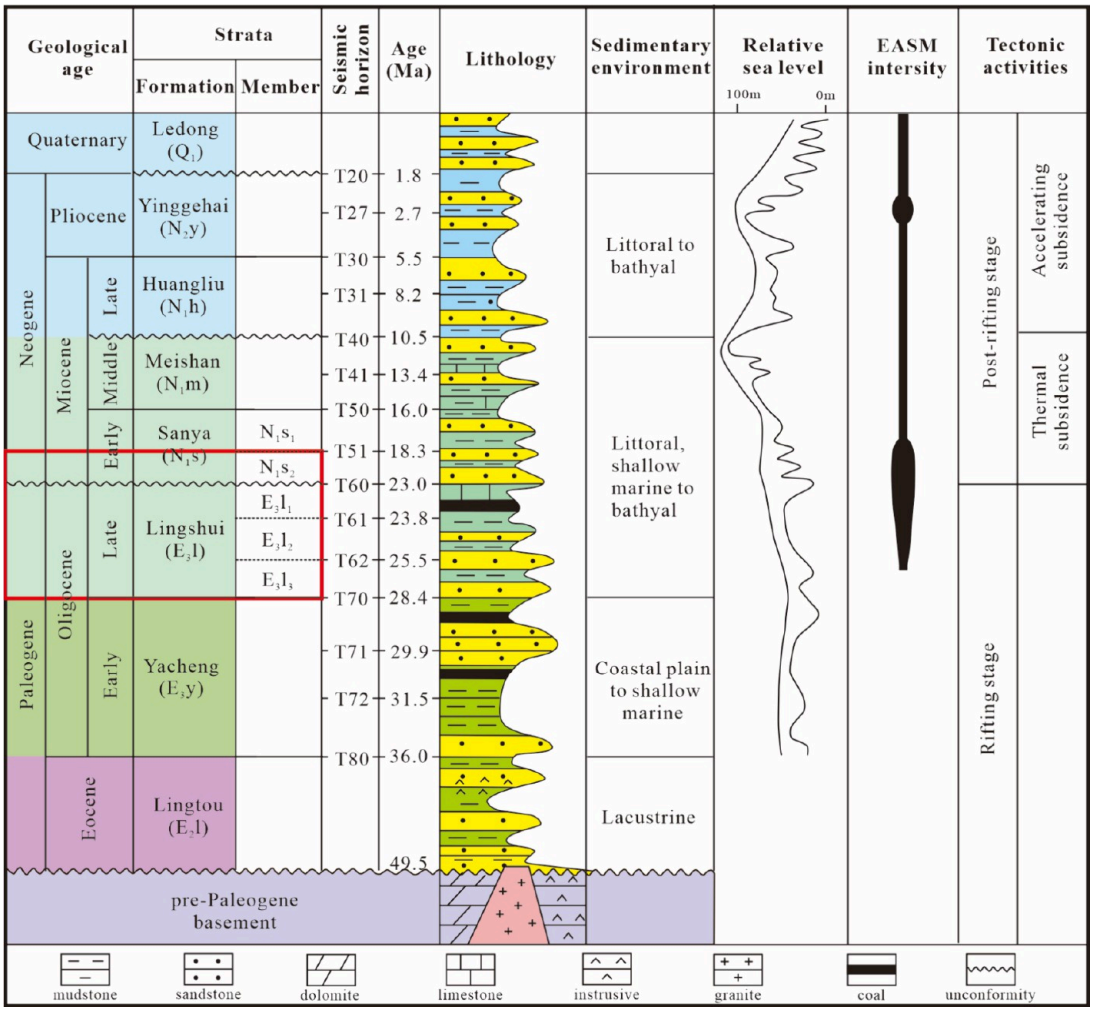

Figure 2. Generalized stratigraphic column of the Qiongdongnan Basin. The age constraints for the studied strata are from Wu.[4] Copyright 2023 American Chemical Society. The global sea level curve was adapted from Xie.[21] Copyright 2008 Elsevier Ltd. The East Asian summer monsoon (EASM) intensity is summarized based on Tada[20] (Copyright 2016 Springer Nature) and Ding[5] (Copyright 2021 Elsevier Ltd.), with the width of the black shape representing the relative intensity of the EASM.

second member of the Lingshui Formation (E_3l_2), and the third member of the Lingshui Formation (E_3l_3). Shallow marine dominates the late Oligocene of the studied area (Figure 3b), while bathyal first occurs in the early Miocene due to the continuous transgression from 28.4 to 10.5 Ma (Figure 2 and Figure 3a). The lithology of our studied samples mainly comprises glutenite, gristone, medium sandstone, fine sandstone, siltstone, pelitic siltstone, silty mudstone, and mudstone/shale. Parts of our target members were influenced by the East Asian summer monsoon (EASM), which has been prevalent since 24.9 Ma ago and continues to the present.[5,20]

3. MATERIALS AND METHODS

The total organic carbon (TOC) and rock pyrolysis data of 692 shale samples obtained from 37 wells (sample data are presented in the Supporting Information), saturated hydrocarbon biomarker data of 60 shale samples obtained from 10 wells that are influenced by deltas (BD1, BD2, BD3, BD4, BD5, BD6, BD7 ST1, ST2, and YC1), and vitrinite reflectance (VR_r%) data of 61 shale samples obtained from 7 wells (BD2, BD3, BD4, BD5, BD7, ST1, and ST2) were involved in this research. The lithological composition of target strata was also statistically analyzed based on the cuttings logging records. It should be mentioned that partial data were supported by the Hainan branch of China National Offshore Oil Corporation (CNOOC).

3.1. TOC and Rock Pyrolysis Analysis. The TOC analysis was performed at the Hainan branch of CNOOC using a LECO CS744 analyzer, preceded by crushing the shale samples to 100 mesh and treating them with HCl to remove carbonate rocks. Rock pyrolysis was performed on a Rock-Eval VI analyzer to obtain parameters such as free hydrocarbon (S_1), pyrolyzed hydrocarbon (S_2), and peak temperature of S_2 (T_{max}). The analytical precision for TOC is 0.01 wt %, while that of S1 and S2 is 0.01 mg/g rock.

3.2. Vitrinite Reflectance Measurement. Chloroform, HCl, and HF were used to eliminate soluble organic matter, carbonate, and silicate rocks for the preparation of kerogen. The vitrinite reflectance measurement of kerogen was conducted at the Hainan branch of CNOOC using an Axio Scope A1-MSP200 microphotometer following the industry standard SY/T 5124-2012. The analytical precision is 0.01%.

3.3. Sporopollen Analysis. Analysis and identification of sporopollen were carried out on a total of 52 shales from well W1 in accord with the industry standard (SY/T 5915-2000) at the Hainan branch of CNOOC. Carbonates and silicates were

https://doi.org/10.1021/acsomega.4c01777
ACS Omega 2024, 9, 22903−22922

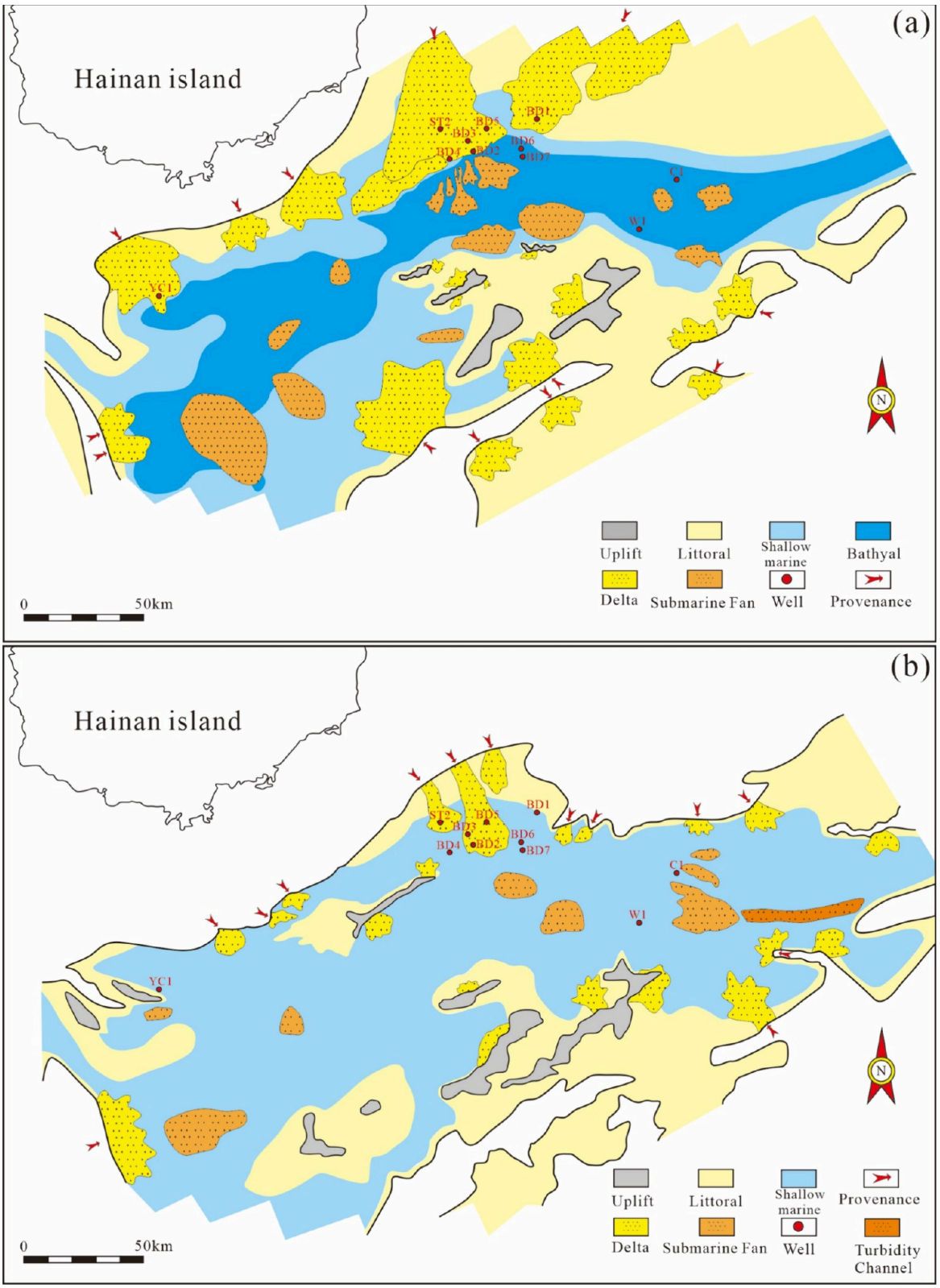

Figure 3. Distributions of sedimentary facies of (a) the second member of the Sanya Formation and (b) the second member of the Lingshui Formation.

eliminated using 10% hydrochloric acid and 40% hydrofluoric acid, respectively. We utilized a heavy liquid (HBr, KI, and Zn) with a specific gravity of 2.0 to separate pollen from the remaining inorganic fraction. Sporopollen were distinguished and counted on a binocular microscope (Leica DM4000B) at 400× magnification. Parallel samples accounted for 5% of the total number of samples, and their color grade index difference was less than 0.25.

3.4. GC-MS Analysis. Saturated fractions were obtained from 60 critical shales by Soxhlet extraction and column

https://doi.org/10.1021/acsomega.4c01777
ACS Omega 2024, 9, 22903−22922

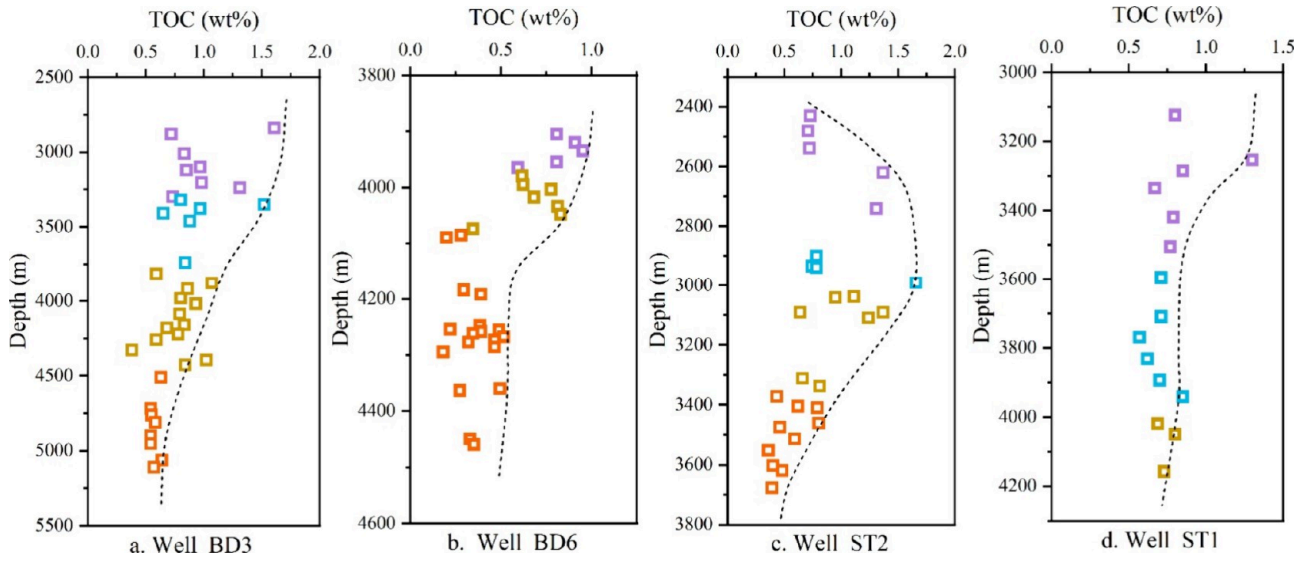

Figure 4. TOC−depth profiles of wells BD3, BD6, ST2, and ST1. The meanings of stratigraphic unit abbreviations are shown in Figure 2, and they remain consistent throughout the following figures and tables. The missing data of E_3l_1 in Well BD6 are caused by strata erosion.

Table 1. Petrographic, Pyrolysis, And Geochemical Data for the Studied Formations[a]

member	TOC (wt %)	$S_1 + S_2$ (mg/g of rock)	HI (mg/g of TOC)	T_{max} (°C)	VR_r (%)	mudstone/shale (%)	silty mudstone (%)	sandstones (%)
N_1s_2	0.17−1.61	0.05−4.4	13−392	412−457	0.51−1.07	62	13	25
	0.68 (227)	1.09 (226)	139 (226)	434 (225)	0.68 (18)			
E_3l_1	0.17−2.32	0.08−5.19	16−447	415−477	0.61−0.78	42	13	45
	0.63 (92)	1.14 (92)	137 (92)	439 (90)	0.66 (16)			
E_3l_2	0.16−1.69	0.02−5.18	2−343	406−463	0.63−1.15	44	10	46
	0.56 (163)	0.89 (162)	107 (162)	437 (136)	0.78 (20)			
E_3l_3	0.16−1.37	0.02−6.75	6−340	401−464	0.72−0.91	30	10	60
	0.51 (210)	0.65 (209)	94 (209)	437 (179)	0.79 (11)			

[a]Note: taking the TOC values of the N_1s_2 as an example, 0.17−1.61 represents the minimum-maximum value, and 0.68 (227) represents the average value (sample numbers). Sandstone contains glutenite, gritstone, medium sandstone, fine sandstone, and siltstone.

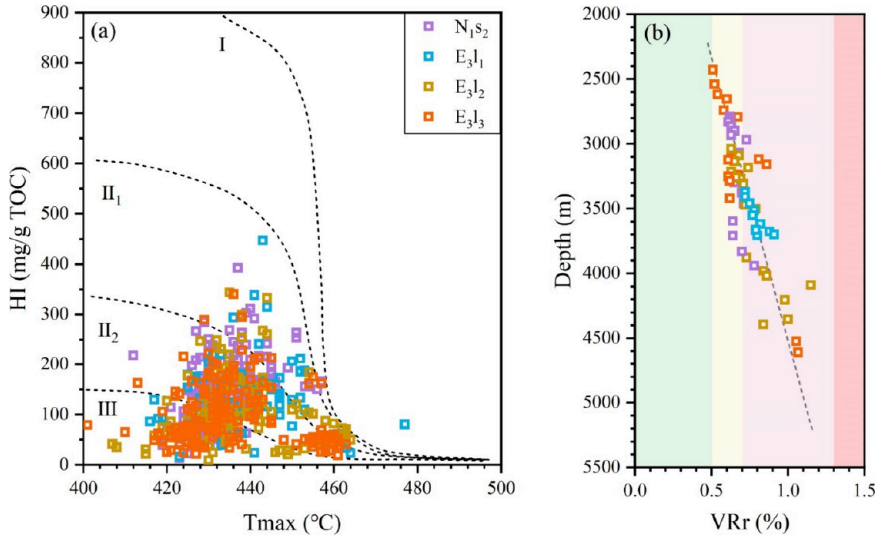

Figure 5. (a) Organic matter type classification based on T_{max} versus HI of a total of 630 shales. (b) VR_r−depth profile of 61 shale samples obtained from 7 wells. The meanings of stratigraphic unit abbreviations are shown in Figure 2.

chromatography. Biomarker analysis of saturated fractions was performed on an Agilent 7890A gas chromatograph coupled to a 5975C mass spectrometer and equipped with an HP-5MS (60 m × 0.25 mm × 0.25 μm) fused silica capillary column at China University of Geosciences, Beijing. Helium was used as the carrier gas, with a constant flow rate of 1.5 mL/min. The GC operating conditions were as follows: the inlet temperature was set to 300 °C, and the oven was heated from 40 to 300 °C at a programed rate of 3 °C/min and then held for 30 min. The

https://doi.org/10.1021/acsomega.4c01777
ACS Omega 2024, 9, 22903−22922

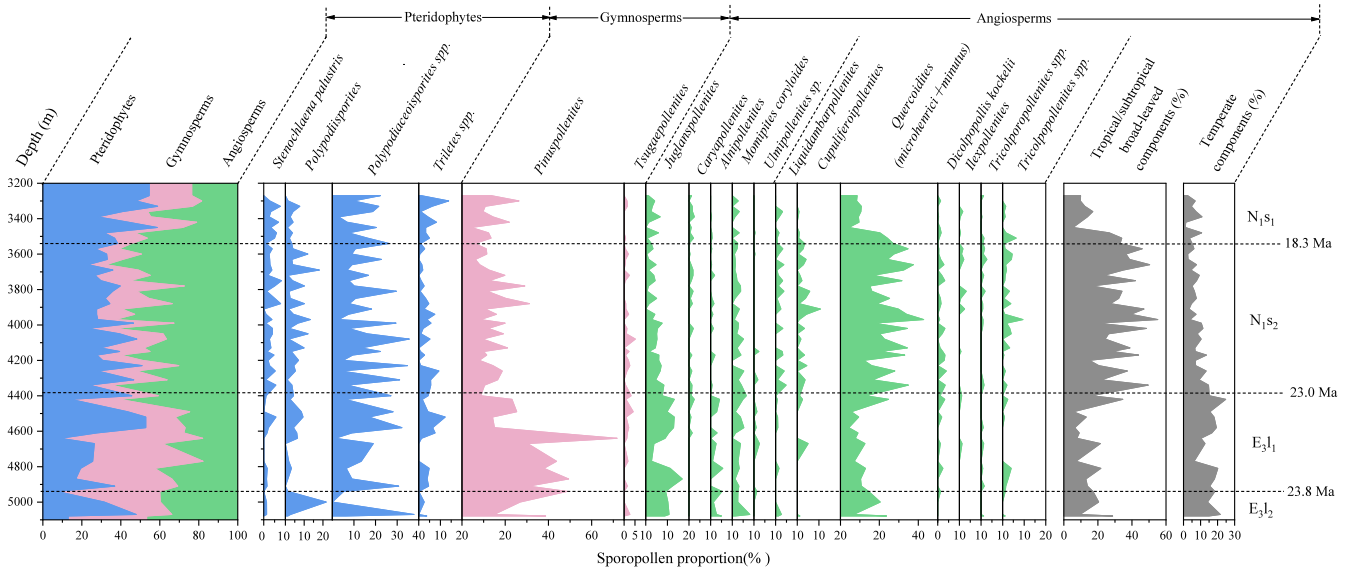

Figure 6. Sporopollen profiles of well W1 in the Qiongdongann Basin. The classification of the tropical/subtropical component and temperate component of angiosperm are primarily based on Ding.[5] Copyright 2021 Elsevier Ltd. The meanings of stratigraphic unit abbreviations are shown in Figure 2.

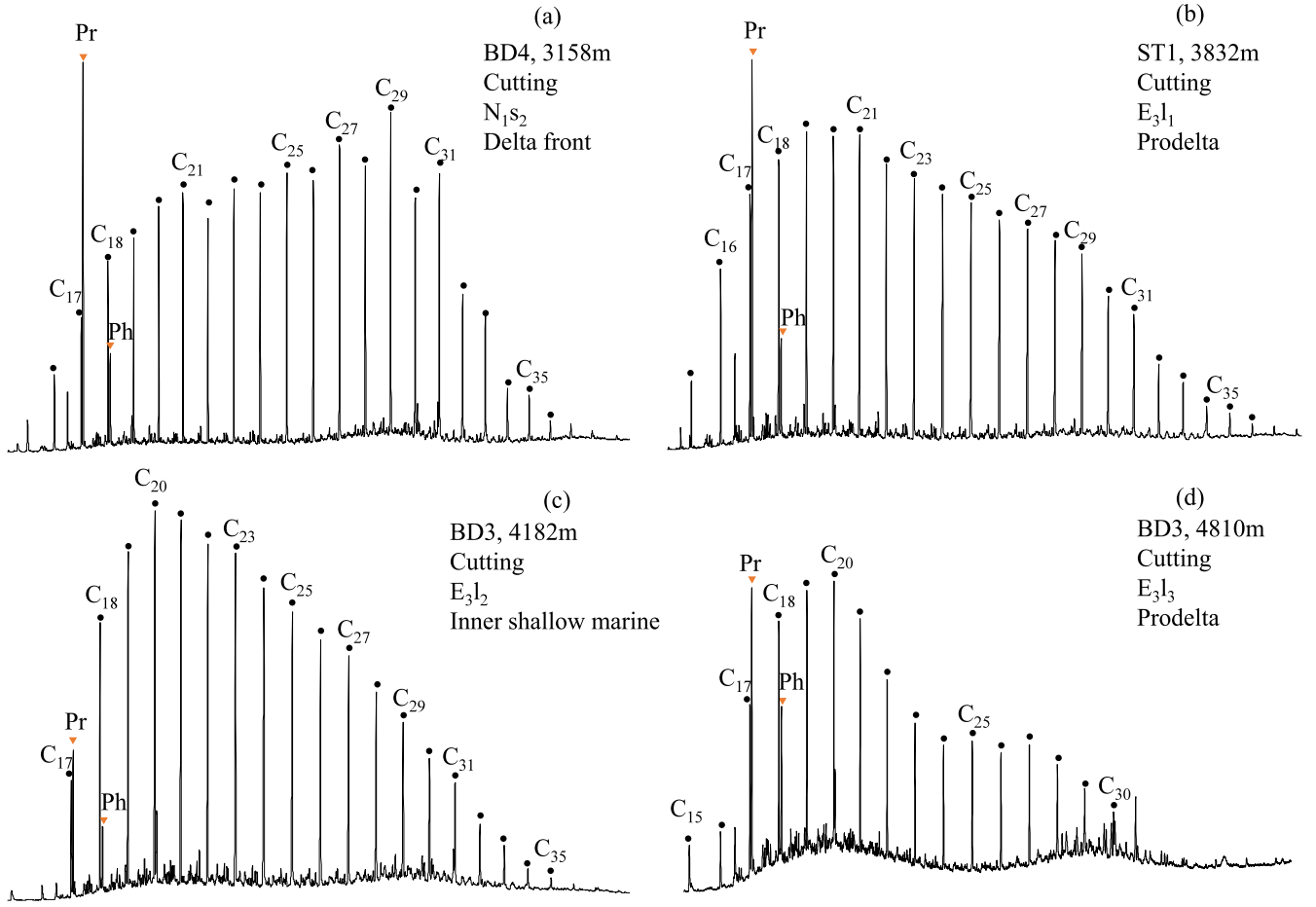

Figure 7. Total ion chromatograms (TICs) of saturated fractions of typical samples from (a) the second member of Sanya Formation, (b) the first member of the Lingshui Formation, (c) the second member of the Lingshui Formation, and (d) the third member of the Lingshui Formation. The four labels consist of well name, sample depth, sample type, stratigraphic unit, and sedimentary facies, the same for Figure 8.

electron ionization energy of the MS ion source was 70 eV. The

signal-to-noise ratio of MS was over 400.

https://doi.org/10.1021/acsomega.4c01777
ACS Omega 2024, 9, 22903−22922

Table 2. Saturated Hydrocarbon Biomarker Parameters of 60 Shale Samples from 10 Wells in the Qiongdongnan Basin[a]

well	depth (m)	Mbr	sample type	subface	P1	P2	P3	P4	P5	P6	P7	P8	P9	P10	P11	P12	P13	P14	P15	P16	P17	TOC (wt %)
BD1	2162	N_1s_2	cutting	delta front	1.07	23.36	0.78	1.32	0.27	1.08	2.18	0.09	0.27	0.02	0.11	1.08	0.55	0.49	0.34	0.73	0.34	0.36
BD1	2190	N_1s_2	cutting	prodelta	1.09	24.72	0.63	2.39	0.33	1.07	2.37		0.35	0.02	0.12	3.54	0.61	0.45	0.91	1.01	0.28	0.36
BD1	2306	E_3l_1	cutting	inner shallow marine	1.22	24.39	0.46	1.58	0.52	1.95	3.43	0.05	0.23	0.01	0.13	1.87	0.35	0.48	0.09	0.75	0.26	0.74
BD2	3040	N_1s_2	cutting	delta front	1.20	24.54	0.47	1.75	0.67	3.66	4.91	0.11	0.62	0.07	0.02	0.32	0.47	0.60	0.17	0.41	0.44	0.56
BD2	3202	N_1s_2	cutting	delta front	1.13	24.62	0.48	1.35	0.46	1.86	4.72	0.17	0.72	0.06	0.01	0.52	0.55	0.60	0.24	1.55	0.44	0.72
BD2	3332	N_1s_2	cutting	delta front	1.11	24.29	0.50	1.55	0.39	1.65	3.48	0.24	1.12	0.07	0.03	0.29	0.48	0.62	0.21			0.81
BD2	3816	E_3l_1	cutting	inner shallow marine	1.00	21.36	0.91	0.30	0.29	1.11	3.37	0.04	0.16	0.02	0.23	0.91	0.56	0.49	0.51	0.80	0.30	0.59
BD2	3820	E_3l_1	cutting	inner shallow marine	1.06	22.09	0.73	0.56	0.36	1.16	2.98	0.08	0.16	0.01	0.18	1.46	0.57	0.49	0.98	1.48	0.30	
BD2	3842	E_3l_1	cutting	inner shallow marine	1.05	22.08	0.75	0.54	0.31	1.27	3.50	0.05	0.11	0.01	0.12	1.32	0.51	0.49	1.43	0.83	0.37	
BD2	3864	E_3l_1	cutting	inner shallow marine	1.03	21.64	0.88	0.37	0.38	1.03	2.09	0.07	0.15	0.01	0.14	1.84	0.53	0.43	0.98	0.84	0.39	
BD2	3886	E_3l_1	cutting	inner shallow marine	1.06	23.09	0.71	0.91	0.24	1.06	3.37	0.22	0.47	0.03	0.13	0.96	0.59	0.58	0.43	0.91	0.46	
BD3	2880	N_1s_2	cutting	delta front	1.24	26.61	0.37	4.23	0.99	6.34	5.35	0.06	0.49	0.10	0.06	0.14	0.34	0.59	0.08	0.63	0.44	0.72
BD3	3100	N_1s_2	cutting	delta front	1.17	26.23	0.39	4.08	0.95	6.26	5.88	0.09	0.44	0.11	0.06	0.19	0.33	0.61	0.20	0.73	0.42	0.97
BD3	3238	N_1s_2	cutting	delta front	1.10	26.30	0.42	4.45	1.05	6.71	5.01	0.13	0.47	0.10	0.05	0.31	0.33	0.60	0.46	0.99	0.39	1.31
BD3	3300	E_3l_1	cutting	delta front	1.11	25.46	0.47	2.45	0.79	4.59	5.16	0.13	0.44	0.15	0.05	0.27	0.39	0.61	1.04	1.15	0.42	0.73
BD3	3380	E_3l_1	cutting	delta front	1.06	25.00	0.52	2.02	0.69	4.30	5.83	0.07	0.22	0.05	0.19	0.22	0.38	0.56	0.30	0.63	0.36	0.97
BD3	3460	E_3l_1	cutting	prodelta	1.07	25.37	0.52	2.63	0.76	3.91	3.93	0.16	0.43	0.11	0.06	0.45	0.48	0.59	0.89	1.01	0.39	0.88
BD3	3878	E_3l_2	cutting	prodelta	1.03	23.96	0.62	1.33	0.27	1.58	4.87	0.08	0.25	0.06	0.15	1.24	0.35	0.53	3.46	0.83	0.40	1.07
BD3	3980	E_3l_2	cutting	prodelta	1.05	24.68	0.59	1.96	0.23	1.20	3.21	0.01	0.09	0.02	0.29	0.25	0.27	0.55	0.85	0.55	0.38	0.8
BD3	4020	E_3l_2	cutting	prodelta	1.04	24.63	0.59	1.77	0.54	3.13	4.17	0.13	0.28	0.11	0.13	0.59	0.38	0.59	2.51	0.71	0.41	0.93
BD3	4092	E_3l_2	cutting	prodelta	1.00	23.64	0.69	1.09	0.17	0.78	3.29	0.03	0.20	0.04	0.07	0.50	0.48	0.56	0.35	0.78	0.30	0.79
BD3	4182	E_3l_2	cutting	prodelta	1.00	23.64	0.68	1.06	0.25	1.22	2.54	0.01	0.08	0.02	0.26	0.31	0.33	0.56	0.52	0.67	0.36	0.68
BD3	4220	E_3l_2	cutting	prodelta	1.01	23.60	0.71	1.31	0.29	1.36	1.47	0.01	0.09	0.02	0.23	0.63	0.35	0.54	0.29	0.61	0.36	0.78
BD3	4330	E_3l_2	cutting	prodelta	1.08	23.65	0.70	1.54	0.54	2.32	1.40	0.01	0.08	0.02	0.15	0.54	0.42	0.53	0.42	0.79	0.35	0.38
BD3	4394	E_3l_2	cutting	prodelta	1.01	23.87	0.57	1.19	0.54	1.09	1.55	0.00	0.08	0.02	0.25	0.46	0.37	0.56	0.05	0.66	0.37	1.02
BD3	4510	E_3l_3	cutting	prodelta	0.98	22.43	0.74	0.67	0.61	1.62	1.91	0.01	0.09	0.03	0.21	0.73	0.44	0.53	0.07	0.80	0.36	0.63
BD3	4718	E_3l_3	cutting	prodelta	0.95	22.18	0.76	0.53	0.83	1.74	1.35	0.01	0.10	0.03	0.22	0.73	0.38	0.54	0.05	0.68	0.36	0.54
BD3	4810	E_3l_3	cutting	prodelta	0.94	21.52	0.78	0.37	0.74	1.73	2.17	0.01	0.07	0.02	0.26	0.75	0.37	0.55	0.08	0.64	0.36	0.58
BD4	3120	N_1s_2	cutting	delta front	1.17	26.43	0.40	3.45	0.99	7.17	5.65	0.10	0.50	0.08	0.05	0.31	0.42	0.59	0.35	0.96	0.33	
BD4	3158	N_1s_2	cutting	delta front	1.18	26.04	0.41	2.91	0.74	5.41	5.05	0.08	0.62	0.08	0.05	0.25	0.46	0.60	0.21	0.85	0.38	
BD5	2655	N_1s_2	cutting	delta front	1.37	26.91	0.34	6.08	1.14	6.63	6.00	0.10	0.22	0.01	0.05	1.27	0.40	0.59	0.08	1.33	0.33	
BD5	2970	E_3l_1	cutting	delta front	1.13	23.71	0.53	1.30	0.41	1.85	3.94	0.07	0.09	0.02	0.07	0.85	0.31	0.60	0.30	0.91	0.40	
BD5	3184	E_3l_2	cutting	prodelta	1.19	25.42	0.54	2.63	0.67	4.52	5.56	0.02	0.14	0.02	0.08	0.94	0.40	0.56	0.67	0.55	0.37	
BD5	3502	E_3l_2	cutting	prodelta	1.14	25.58	0.51	2.93	0.39	1.85	3.51	0.04	0.13	0.01	0.12	0.78	0.46	0.55	0.45	0.98	0.43	0.35
BD5	3708	E_3l_3	cutting	prodelta	1.09	24.19	0.62	1.47	0.28	0.89	2.49	0.03	0.07	0.00	0.12	0.76	0.53	0.56	0.01	1.29	0.36	
BD6	4254.5	E_3l_3	sidecore	delta front	0.99	22.75	0.66	0.53	0.40	0.87	2.10	0.08	0.48	0.09	0.10	0.90	0.55	0.48	0.68	1.01	0.45	0.22
BD7	4034.4	N_1s_2	sidecore	delta front	1.19	27.32	0.35	10.71	0.92	4.09	3.91	0.23	1.10	0.24	0.12	0.16	0.53	0.57	0.52	1.08	0.43	
BD7	4038	N_1s_2	sidecore	delta front	1.23	26.27	0.38	5.08	0.93	5.33	5.06	0.16	0.93	0.20	0.10	0.11	0.56	0.58	0.18	1.15	0.43	0.84

https://doi.org/10.1021/acsomega.4c01777
ACS Omega 2024, 9, 22903−22922

Table 2. continued

well	depth (m)	Mbr	sample type	subface	P1	P2	P3	P4	P5	P6	P7	P8	P9	P10	P11	P12	P13	P14	P15	P16	P17	TOC (wt %)
BD7	4044	N_1s_2	sidecore	delta front	1.08	24.31	0.56	1.90	0.80	4.95	4.67	0.40	1.34	0.25	0.11	0.20	0.56	0.59	0.92	1.18	0.41	
BD7	4062.4	N_1s_2	sidecore	prodelta	1.09	23.75	0.80	2.07	1.10	3.09	2.54	0.17	0.66	0.13	0.11	0.33	0.29	0.50	1.08	0.59	0.28	
ST1	3286	N_1s_2	cutting	inner shallow marine	1.13	26.08	0.45	3.75	0.96	4.26	3.52	0.10	0.60	0.10	0.03	0.29	0.40	0.59	0.47	0.61	0.42	0.85
ST1	3336	N_1s_2	cutting	inner shallow marine	1.13	26.56	0.42	5.34	1.00	5.10	3.24	0.09	0.62	0.07	0.07	0.20	0.45	0.59	0.27	0.41	0.42	0.67
ST1	3832	E_3l_1	cutting	inner shallow marine	1.07	23.86	0.62	1.17	0.47	2.20	4.20	0.12	0.42	0.09	0.11	0.62	0.45	0.51	2.37	0.43	0.42	0.62
ST1	3942	E_3l_1	cutting	inner shallow marine	1.04	23.80	0.66	1.25	0.29	1.70	4.65	0.09	0.39	0.09	0.12	1.10	0.48	0.55	1.83	0.60	0.43	0.85
ST1	4020	E_3l_2	cutting	delta front	1.07	24.54	0.60	1.80	0.34	1.57	3.89	0.13	0.46	0.09	0.06	0.84	0.59	0.57	0.70	0.60	0.38	0.69
ST1	4050	E_3l_2	cutting	prodelta	1.08	24.90	0.65	3.21	0.41	2.05	1.48	0.02	0.13	0.04	0.13	0.56	0.51	0.53	0.50	0.57	0.40	0.8
ST1	4158	E_3l_2	cutting	prodelta	1.08	25.02	0.60	3.34	0.40	1.68	1.31	0.01	0.11	0.03	0.14	0.40	0.47	0.56	0.18	0.53	0.40	0.73
ST2	2540	N_1s_2	cutting	delta front	1.33	25.04	0.41	1.85	0.38	2.21	2.83	0.10	0.20	0.01	0.04	0.80	0.27	0.57	0.26	0.57	0.35	0.72
ST2	2754	N_1s_2	cutting	delta front	0.93	27.68	0.41		0.81		2.41	0.08	0.13	0.02	0.03	0.34	0.41	0.62	0.42	0.37		
ST2	2764	E_3l_1	cutting	delta front	0.93	26.25	0.60	8.14	0.69	8.07	2.69	0.14	0.32	0.02	0.03	0.78	0.33	0.62	0.42	0.29	0.39	
ST2	2778	E_3l_1	cutting	delta front	0.93	26.04	0.62	6.29	0.74	8.60	2.99	0.12	0.19	0.04	0.02	0.91	0.25	0.61	1.51	0.42	0.34	
ST2	2814	E_3l_1	cutting	delta front	1.13	25.27	0.61	4.88	0.42	2.46	2.62	0.13	0.27	0.02	0.03	0.76	0.34	0.61	0.52	0.41		
ST2	2832	E_3l_1	cutting	prodelta	1.17	26.95	0.37	9.15	0.36	3.34	5.06	0.06	0.13	0.02	0.02	0.17	0.34	0.58	1.58	0.37	0.47	
ST2	3214	E_3l_2	cutting	prodelta	1.23	27.20	0.32	5.54	0.76	4.98	4.33	0.08	0.17	0.01	0.02	0.34		0.59	0.87	0.43	0.43	
ST2	3462	E_3l_3	cutting	inner shallow marine	1.15	23.97	0.57	1.32	0.46	1.89	2.86	0.09	0.26	0.06	0.12	2.79	0.49	0.51	0.93	0.80		0.8
ST2	3552	E_3l_3	cutting	inner shallow marine	1.11	24.63	0.55	1.75	0.39	1.33	2.42	0.03	0.23	0.04	0.11	0.90	0.48	0.56	0.95	1.07	0.43	0.36
ST2	3678	E_3l_3	cutting	inner shallow marine	1.07	23.47	0.68	1.09	0.23	0.77	1.69		0.16	0.03	0.08	2.21	0.46	0.46	0.55	0.99		0.39
YC1	3838	E_3l_1	cutting	prodelta	1.12	25.43	0.52	2.88	0.41	2.11	2.51	0.10	0.22	0.06	0.05	0.23	0.56	0.54	1.13	0.57		0.65
YC1	3972	E_3l_2	cutting	inner shallow marine	1.11	24.33	0.59	1.46	0.59	1.58	1.68	0.04	0.10	0.03	0.18	0.53	0.52	0.42	0.33	0.91		0.45
YC1	4158	E_3l_2	cutting	inner shallow marine	1.09	23.99	0.63	1.23	0.34	1.16	2.29	0.03	0.13	0.00	0.00	0.80	0.50	0.34	1.13	1.08		0.58

[a]Note: P1 is CPI, calculated through $2 \times (C_{23} + C_{25} + C_{27} + C_{29} + C_{31})/(C_{22} + 2C_{24} + 2C_{26} + 2C_{28} + 2C_{30} + C_{32})$ *n*-alkanes;[26] P2 is ACL, calculated through $(25 \times C_{25} + 27 \times C_{27} + 29 \times C_{29} + 31 \times C_{31} + 33 \times C_{33})/(C_{25} + C_{27} + C_{29} + C_{31} + C_{33})$ *n*-alkanes;[27] P3 is P_{aq}, calculated through $(C_{23} + C_{25})/(C_{23} + C_{25} + C_{29} + C_{31})$ *n*-alkanes;[24] P4 is TAR, calculated through $(C_{27} + C_{29} + C_{31})/(C_{15} + C_{17} + C_{19})$ *n*-alkanes;[28] P5 is Ph/*n*-C_{18}; P6 is Pr/*n*-C_{17}; P7 is Pr/Ph; P8 is des-A-oleanane/C_{30}H; P9 is oleanane/C_{30}H; P10 is taraxerane/C_{30}H; P11 is gammacerane/C_{30}H; P12 is TT/C_{30}H, where TT contains C_{19}−C_{26} tricyclic terpanes; P13 is Ts/(Ts + Tm); P_{14} is C_{31} $\alpha\beta$-hopane-22S/(22S + 22R); P15 is T/C_{30}H; P16 is C_{27}/C_{29} $\alpha\alpha\alpha$ 20R sterane; P17 is C_{29} $\alpha\alpha\alpha$ sterane-20S /(20S + 20R). Mbr represents member; Pr represents pristane; Ph reprents phytane; C_{30}H represents C_{30} $\alpha\beta$-hopane; T represents *trans-trans-trans*-bicadinane; Ts and Tm represent C_{27} 18 $\alpha(H)$-22,29,30-trisnorneohopane and C_{27} 17 $\alpha(H)$-22,29,30-trisnorneohopane, respectively. Parameters P1−P7, P8−P14, P15, and P16 and P17 were determined based on the peak areas on the TIC, *m*/*z* 191, *m*/*z* 412, and *m*/*z* 217 mass chromatograms of the saturated fractions, respectively.

https://doi.org/10.1021/acsomega.4c01777
ACS Omega 2024, 9, 22903−22922

4. RESULTS

4.1. Bulk Geochemical Parameters. Both TOC and S_1 + S_2 are typical parameters indicating organic matter abundance. The third member of the Lingshui Formation had the lowest TOC and $S_1 + S_2$, with average values of 0.51% and 0.65 mg/g of rock, respectively. Shales from the second member of the Sanya Formation showed the highest TOC (0.17−1.61%, average 0.68%), while the first member of the Lingshui Formation has the highest $S_1 + S_2$ (0.08−5.19 mg/g rock, average 1.14 mg/g rock). It is obvious that there is an increasing trend in TOC from the third member of the Lingshui Formation to the second member of the Sanya Formation roughly, as shown in Figure 4 and Table 1.

The hydrogen index (HI), commonly employed as an indicator of organic matter type, reflects the potential of hydrocarbon generation and is defined as the ratio of $S_1 + S_2$ to TOC. Samples from the third Lingshui Formation had the lowest HI (6−340 mg/g of TOC, average 94 mg/g of TOC), while the highest value (16 to 447 mg/g of TOC, 137 mg/g of TOC) was observed in the first member of the Lingshui Formation.

The T_{max} of these shales varied from 401 to 477 °C, and there were no remarkable differences in average values among the four target members. The vitrinite reflectance (VR_t%) of most analyzed samples fell in the range of 0.51−1.15%, with the majority being in the low to moderately mature stage (Figure 5b). According to the typical HI versus T_{max} plate (Figure 5a), these samples were mainly classified as type II_2−III organic matter, with only a small number of samples falling within the zone of type II_1.

4.2. Sporopollen Composition. A total of 85 fossil taxa were identified in samples from well W1, including 20 taxa of pteridophytes, 9 taxa of gymnosperms, and 56 taxa of angiosperms. The pollen of angiosperms accounted for 14−65%, with an average of 38.3%; the main taxa included *Quercoidites* (*microhenrici* and *minutus*), *Juglanspollenites*, and *Momipites coryloide*, while *Alnipollenites*, *Caryapollenites*, *Ulmipollenites sp.*, *Liquidambarpollenites*, *Cupuliferoipollenites*, *Dicolpopollis kockelii*, *Ilexpollenites*, *Tricolporopollenites spp.*, and *Tricolpopollenites spp.* were commonly observed. Pteridophyte spores made up a significant proportion of these fossil taxa, ranging from 6.6% to 52.8%, with an average of 30.5%. The majority of pteridophyte taxa were *Polypodiaceoisporites spp.* (0−40%, average 19.9%), *Polypodiisporites* (0−21.8%, average 5.9%), *Triletes spp.* (0−13.9%, average 13.4%), and *Stenochlaena palustris* (0−8.2%, average 2.8%). The relative content of gymnosperm taxa varied greatly from 7.9% to 73.1% with an average of 21.5%, and they were dominated by *Pinuspollenites* (4.3−71.8%, average 19.9%), followed by *Tsugaepollenites* (0−5.2%, average 1.0%).

Based on the ecological adaptations of different vegetation reported in previous research,[5] these genera and families of angiosperms could be classified into tropical/subtropical broad-leaved taxa and temperate taxa. The tropical/subtropical broad-leaved taxa in well W1 were mainly comprised of *Juglanspollenites*, *Caryapollenites*, *Alnipollenites*, *Momipites coryloides*, and *Ulmipollenites sp.*, while the temperate taxa consisted of *Liquidambarpollenites*, *Cupuliferoipollenites*, *Quercoidites* (*microhenrici* and *minutus*), *Dicolpopollis kockelii*, *Ilexpollenites*, *Tricolporopollenites spp.*, *and Tricolpopollenites spp.* Both *Pinuspollenites* and *Tsugaepollenites* in gymnosperms belonged to mountainous conifers taxa. Samples in the first and second members of the Lingshui Formation were characterized by a low content of pteridophytes, a low content of tropical/subtropical broad-leveled taxa, and a high content of temperate taxa, suggesting a relatively cool and dry climate. On the contrary, these shales in the second member of the Sanya Formation were dominated by tropical/subtropical broad-leveled taxa and pteridophytes, while the proportion of temperate taxa and *Pinuspollenites* decreased sharply (Figure 6), implying a warm and humid climate during 23−18.3 Ma.

4.3. *n*-Alkanes and Isoprenoids. The unimodal distribution pattern dominates the *n*-alkane distribution, but there is a wide range for the main peak carbon of these samples (Figure 7). Shales from the second member of the Sanya Formation was predominantly characterized by a relatively high abundance of *n*-C_{25}, *n*-C_{27}, and *n*-C_{29} (Figure 7a). The main peak positions shifted toward low-carbon-number (<25) *n*-alkanes in the Lingshui Formation compared with the second member of the Sanya Formation (Figure 7), but no remarkable main peaks were observed in the first member of the Lingshui Formation. Low-carbon-number *n*-alkanes (the main peak below *n*-C_{23}) were relatively abundant in the third member of the Lingshui Formation (Figure 7d). Normally, long-chain *n*-alkanes with *n*-C_{27}, *n*-C_{29}, or *n*-C_{31} predominance indicate terrigenous plants, with *n*-C_{15}, *n*-C_{17}, or *n*-C_{19} predominance mainly derived from algae sources.[22,23] *n*-C_{21}, *n*-C_{23}, and *n*-C_{25} are associated more with aquatic macrophytes.[24] The carbon preference index (CPI, definition in Table 2) was used to determine the organic matter sources and thermal maturity, since a value approaching 1.0 indicates the input of marine microorganisms and/or recycled organic matter, suggesting a mature thermal stage.[25,26] The CPI of these samples ranged from 0.93 to 1.37, with a mean value of 1.09. Shales from the Lingshui Formation showed a similar CPI value (<1.1) with minor variations. As for the shallowest buried shales from the second member of the Sanya Formation, the average CPI value was 1.15, with two samples reaching 1.33 and 1.37.

The average chain length of *n*-alkanes (ACL, definition in the note of Table 2) is lower in marine organic matter (14−24) while higher in terrigenous organic matter (21−39).[27] The terrigenous to aquatic ratio (TAR, definition in the note of Table 2) was also proposed to reflect the source composition of sediments.[28] From bottom to top of our target members, the average TAR increased from 0.97 to 3.57, while the average ACL increased from 23.1 to 25.64, reflecting the stepwise growing input of terrestrial higher plants. The P_{aq} (definition in the note of Table 2) is used to evaluate the nonemergent aquatic macrophyte input relative to that from the emergent aquatic and terrestrial plants.[24] Low P_{aq} values were observed in the studied shales, ranging from 0.32 to 0.91 (average 0.57). Among them, samples from the third Lingshui Formation showed the highest P_{aq} value at 0.67. The variation trend of P_{aq} across different target members was the opposite of that of ACL and TAR, also suggesting a gradual increase in the contribution of terrestrial higher plants from the third member of the Lingshui Formation to the second member of the Sanya Formation.

The pristane/phytane (Pr/Ph) ratio lies in a wide range (1.31−6.00, average 3.41), and there was considerable variation in the average values among different formations. Shales in the third member of the Lingshui Formation exhibited the lowest average Pr/Ph at 2.12, while the highest average value of 4.15 was observed in the second member of the Sanya Formation. Pr/*n*-C_{17} in these samples ranged from 0.77 to 8.6, with an average

https://doi.org/10.1021/acsomega.4c01777
ACS Omega 2024, 9, 22903−22922

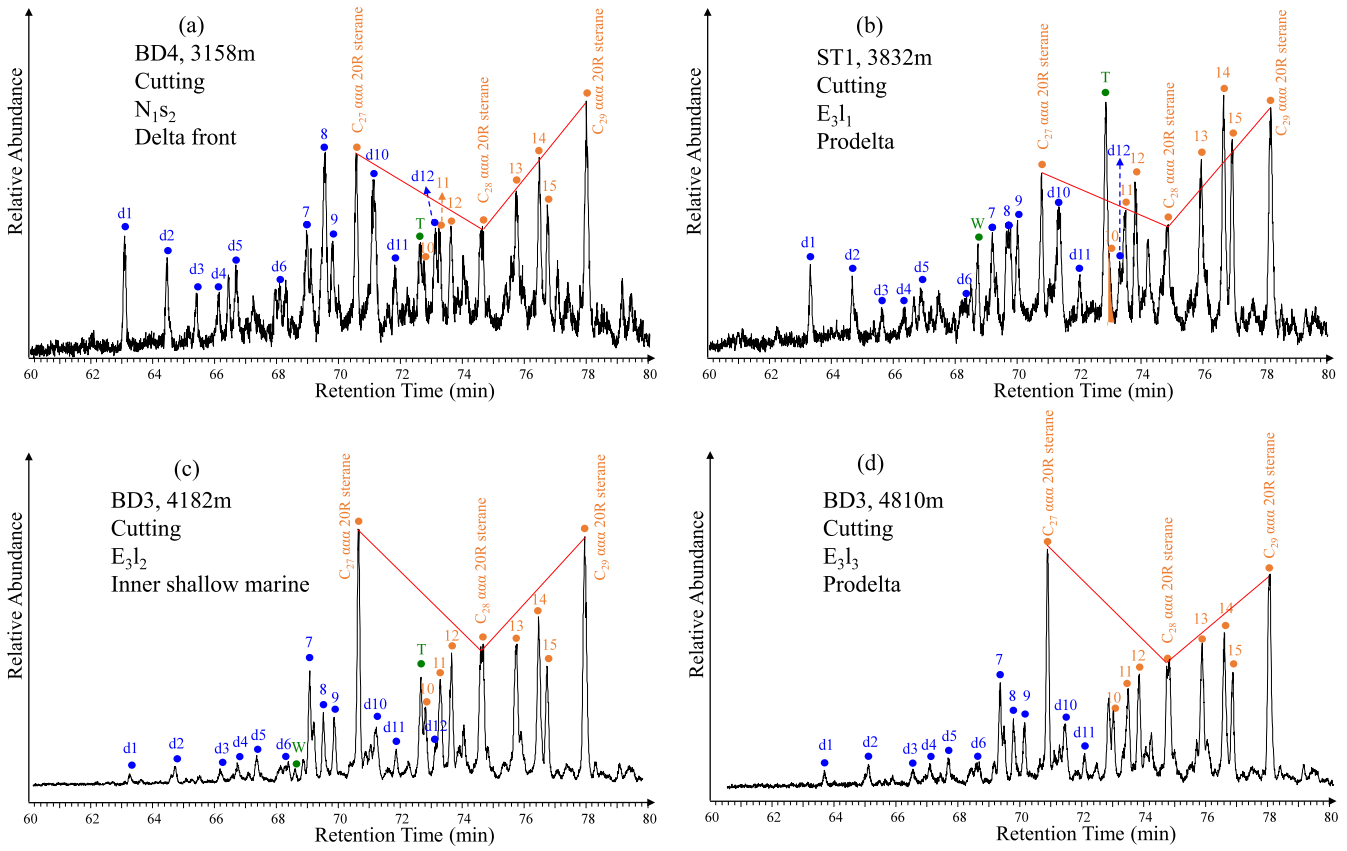

Figure 8. Partial mass chromatogram at *m*/*z* 217 showing the distributions of the steroids in typical samples from (a) the second member of Sanya Formation, (b) the first member of the Lingshui Formation, (c) the second member of the Lingshui Formation, and (d) the third member of the Lingshui Formation. Peaks d1−d12 are C_{27}−C_{29} diasteranes, peaks 7−9 are the mixtures of diasteranes and C_{27} regular steranes, peaks 10−12 are C_{28} regular steranes, and peaks 13−15 are C_{29} regular steranes. Compounds W and T are bicadinanes.

of 2.89, while Ph/*n*-C_{18} ranged from 0.17 to 1.14, with an average of 0.56.

4.4. Steroids. The regular distribution pattern of steranes serves as a commonly used biological sources indicator.[29,30] Both complete regular and rearranged steranes were detected in these samples (Figure 8). The C_{27}/C_{29} *ααα* 20R steranes ranged from to 0.29 to 1.55 with an average 0.78. Most of samples in the first and second members of the Lingshui Formations, and the second member of the Sanya Formation exhibited a prevalence pattern of C_{29} over C_{27} regular steranes (Figure 8a−c), indicating the main contribution of terrigenous organic matter.[29] However, a slight prevalence of C_{27} over C_{29} regular steranes was observed in the third member of the Lingshui Formation, implying the important source of aquatic organisms (Figure 8d).

The isomerization degree of steranes is a widely applied maturity-related parameter.[31] The C_{29}-*ααα* 20S/(20S+20R) ratios of the 60 samples have not reached equilibrium (0.26 to 0.47, average 0.38), corroborating the measured maturity of VR_r% presented in Figure 5b.

4.5. Terpenoids. Abundant terpenoids were identified in the *m*/*z* 191 and 412 mass chromatograms, including tricyclic terpanes, C_{27}−C_{35} hopanes, bicadinanes, oleanane and its derivatives (X, Y, Z, and Z1), rearranged oleananes, taraxerane, and gammacerane.

The tricyclic terpanes (TTs) primarily contained C_{19}−C_{26}TT, with the main peaks being C_{21} or C_{23}TT (Figure 9). This distribution pattern reflected algal sources, specifically associated more on Tasmania algae.[32] The TT/C_{30}H ratio was used to characterize the relative abundance of tricyclic terpanes in this research, ranging from 0.11 to 3.54 with an average of 0.74. While the abundances of tricyclic terpanes in the second member of the Sanya Formation and the first and second members of the Lingshui Formations were similar (Figure 9a−c), there was a significantly higher TT/C_{30}H ratio in the third member of the Lingshui Formation (average 1.22) (Figure 9d).

Hopanes are believed to derive from bacteriohopaneterol in prokaryotic organisms.[33] The distribution of hopanes in the studied shales was dominated by C_{27}−C_{31} hopanes, with a decreasing trend of C_{32}−C_{35} homohopanes (Figure 9). The maturity parameter Ts/(Ts + Tm) ranged from 0.25 to 0.61, with an average of 0.43. Another maturity indicator, C_{31} *αβ* hopane-22S/(22S + 22R), ranged from 0.34 to 0.62, with an average of 0.55. Thermal maturation was determined to be from a low to moderately mature stage through hopane parameters, with minor differences among members, consistent with the characteristics of CPI, sterane isomerization parameters, and measured VR_r%.

Oleanane-type terpanes are comprised of oleanane, rearranged oleanane, des-A-oleanane, X, Y, Z, and Z1, serving as credible angiosperm indicators in tertiary sediments, and they can be identified in the *m*/*z* 191 mass chromatogram.[34−37] Oleanane was detected in most samples with great fluctuations, and the oleanane/C_{30}H ratio ranged from 0.07 to 1.34, with an average of 0.33. The highest average value of oleanane/C_{30}H (0.63) occurred in the second member of the Sanya Formation (Figure 9a). Des-A-oleanane was thought to be derived from the corresponding triterpanes.[34] The highest average value of des-A-

https://doi.org/10.1021/acsomega.4c01777
ACS Omega 2024, 9, 22903−22922

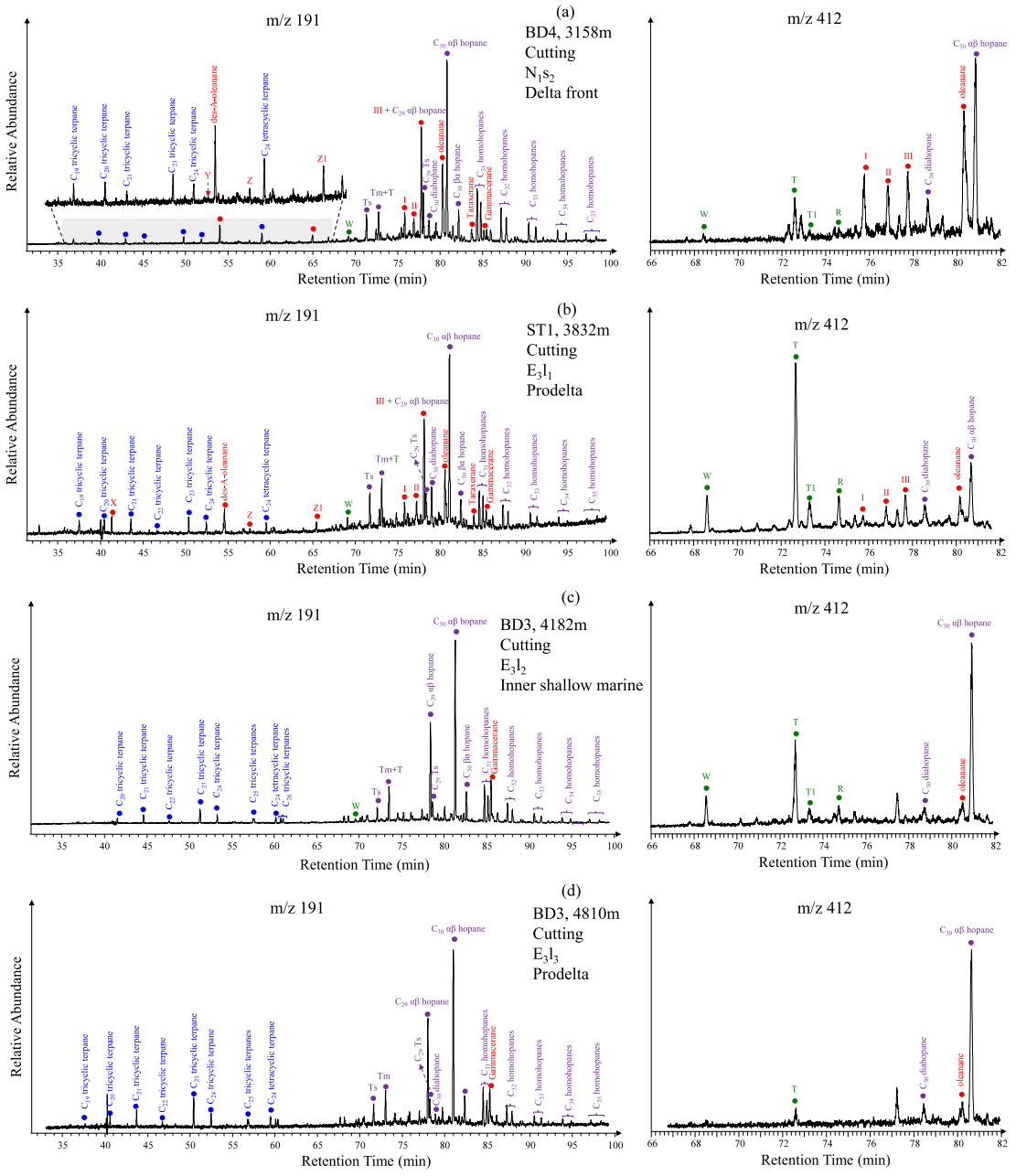

Figure 9. Partial mass chromatograms at m/z 191 and m/z 412 showing the distributions of the terpanes in typical samples from (a) the second member of Sanya Formation, (b) the first member of the Lingshui Formation, (c) the second member of the Lingshui Formation, and (d) the third member of the Lingshui Formation. Compounds I, II, and III are determined to be rearranged oleananes.[36] Copyright 2010 Elsevier Ltd. Compounds X, Y, Z, and Z1 are triterpanes and derived from oleananes.[37] Copyright 2010 Elsevier Ltd. Compounds W, T, T1, and R are bicadinanes.

oleanane/C_{30}H occurred in the second member of the Sanya Formation. X, Y, Z, and Z1 compounds are derived from the oleanane through the cleavage of rings A and B. They were identified as C_{21}, C_{25} triterpanes, and C_{27} tetraterpanes, and were initially reported in the Niger Basin.[37] Although X, Y, Z, and Z1 could be recognized in the m/z 191 mass chromatogram for most samples, their abundances were generally low. Both rearranged oleananes and oleanane originate from functionalized oleanane triterpenoids but follow different diagenetic pathways.[36,38] Rearranged oleananes were identified in the m/z 412 mass chromatogram, since compound III normally coelutes with C_{29} $\alpha\beta$ hopane in the m/z 191 mass chromatogram (Figure 9). The relative abundances of rearranged oleananes (I, II, and III) were usually low in the majority of these samples and were mainly controlled by the depositional environment rather than maturity.[39] As a result of the low content of X, Y, Z, Z1, and rearranged oleananes, oleanane/C_{30}H was used to reflect the abundance of oleanane-type terpanes in this Article.

Bicadinanes are another typical triterpane detected in the Qiongdongnan Basin, mainly originating from Dammer resins of the *Dipterocarpaceae* angiosperm family.[40] Four isomers of bicadinanes (W, T, R, and R1) were identified in the m/z 412 mass chromatogram (Figure 9). Because of the predominance of compound T in all bicadinanes, the T/C_{30}H ratio was used to access the relative concentration of total bicadinanes. The T/C_{30}H ratio in these shale samples varied widely, ranging from 0.01 to 3.46, with an average of 0.67.

https://doi.org/10.1021/acsomega.4c01777
ACS Omega 2024, 9, 22903−22922

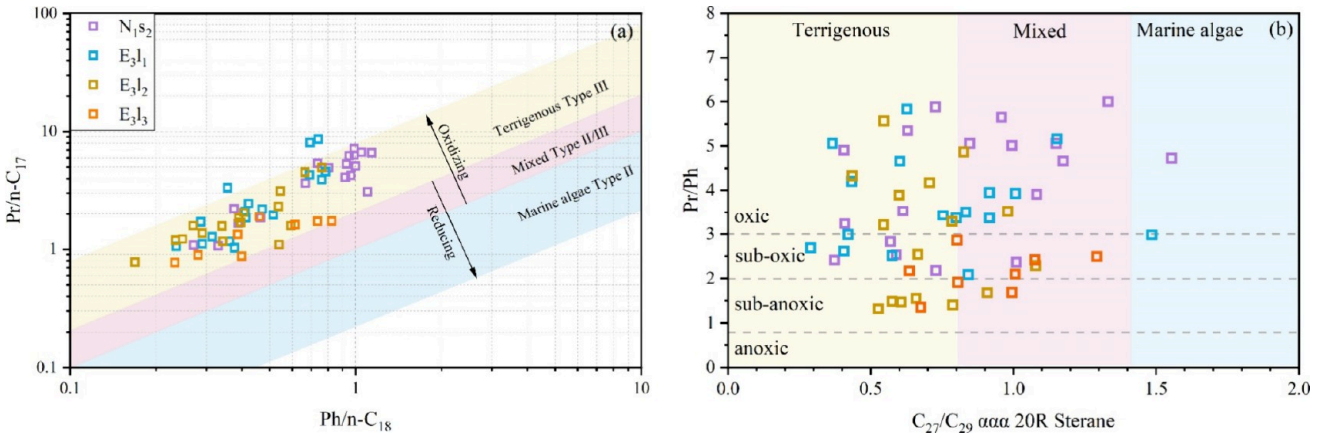

Figure 10. Cross plots of (a) Pr/*n*-C_{17} versus Ph/*n*-C_{18} (from Shanmugam[44]) and (b)Pr/Ph versus C_{27}/C_{29} *ααα* 20R sterane (from Ding[1]), showing the organic matter type and environment. The meanings of stratigraphic unit abbreviations are shown in Figure 2.

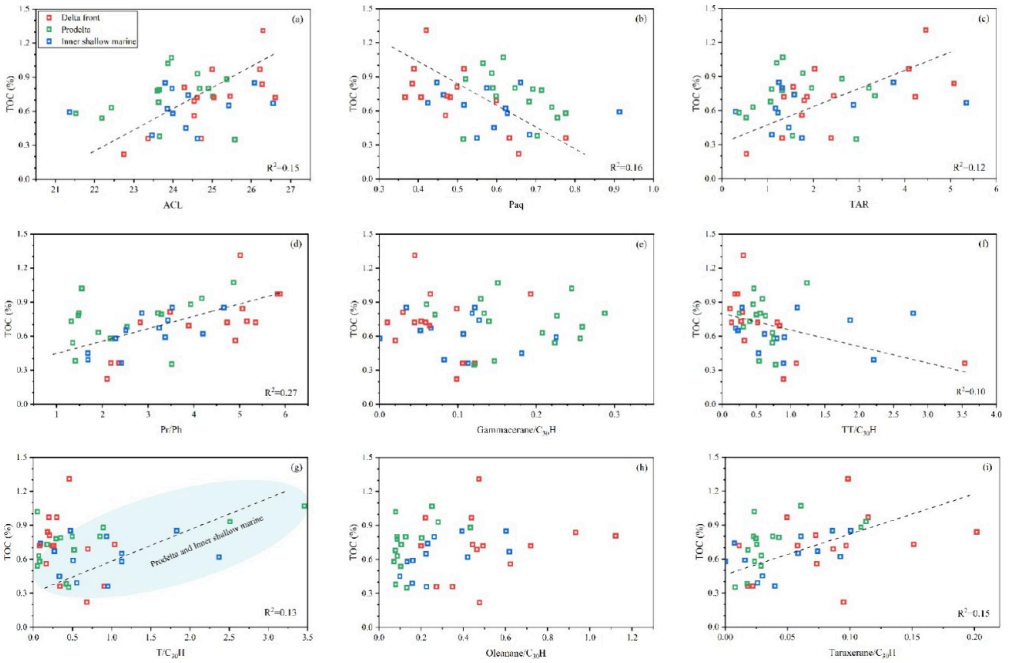

Figure 11. Cross plots of TOC against multiple saturated hydrocarbon biomarker parameters (a) ACL, (b) P_{aq}, (c) TAR, (d) Pr/Ph, (e) gammacerane/C_{30}H, (f) TT/C_{30}H, (g) TT/C_{30}H, (h) oleanane/C_{30}H, and (i) taraxerane/C_{30}H. The definitions of these biomarker parameters are given in the footnote of Table 2. Samples from different sedimentary facies are distinguished by different colors.

Other nonhopanoid triterpanes such as taraxerane and gammacerane were also detected. Angiosperm, especially mangrove vegetation, was thought to be the biological precursor of high-content taraxerane.[41] The taraxerane/C_{30}H in the studied shales ranged from 0 to 0.25, with an average of 0.06. Gammacerane is an indicator of water column stratification and salinity.[42] The distribution of gammacerane in these shales ranged from 0.29, with an average of 0.11.

5. DISCUSSIONS

5.1. Depositional Environment and Source Type. From oxidation to reduction, the redox conditions of the water column are usually divided into oxic, suboxic, subanoxic, anoxic, and euxinic in this Article. The depositional environment of shales in this study is primarily assessed by commonly used Pr/Ph, where a ratio greater than 3.0 reflects oxidized depositional environments and that less than 0.8 reflects reduced environments.[26] The distribution of Pr/Ph in Figure 10 shows slight differences in the depositional environments among these members. The majority of our studied samples were deposited under oxic to suboxic conditions, whereas a minority of samples from the second and third members of the Lingshui Formation fall within the subanoxic zone. The plot of Pr/*n*-C_{17} versus Ph/*n*-C_{18} is also an effective tool for determining organic matter type.[43−45] As shown in Figure 10a, most of the samples are located in the terrigenous type III zone, indicating a predominant contribution from terrigenous organic matter. This feature is further supported by the wide occurrence of oleanane-type terpanes and bicadinanes. However, some shales from the third member of the Lingshui Formation are classified in the mixed type II/III zone, suggesting a significant contribution from marine organic materials. C_{27} steroids are considered to be primarily derived from Rhodophyta.[46] The relatively higher C_{27}/C_{29} *ααα* 20R sterane (average 0.91) in samples from the third member of the Lingshui Formation matches the distributions of *n*-alkanes

https://doi.org/10.1021/acsomega.4c01777
ACS Omega 2024, 9, 22903−22922

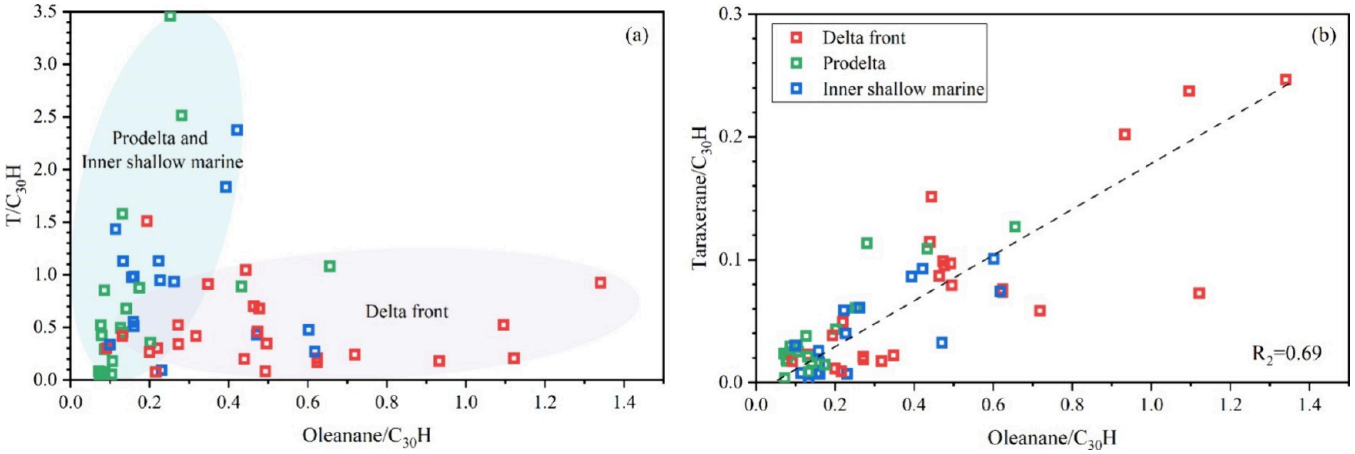

Figure 12. Cross plots of (a) $T/C_{30}H$ and (b) taraxerane/$C_{30}H$ against oleanane/$C_{30}H$ ratios. Samples from different sedimentary facies are distinguished by different colors.

(Figure 7d) and tricyclic terpanes (Figure 9d), implying the increasing input of marine algae.

Generally, our studied shales were primarily deposited under oxic to suboxic conditions, while minor samples were deposited under subanoxic condition. Moreover, from bottom to top of our target strata, the oxidation of the water column is generally enhanced. Influenced by the delta-marginal sea system, the organic materials preserved in these marine source rocks are contributed by both terrestrial higher plants and marine algae, with terrestrial organic matter being the major component. It should be mentioned that samples in the third member of the Lingshui Formation received more marine algae materials than the others.

5.2. Determination of Efficient Source Biomarker Parameters. We attempt to develop a method for calculating the proportion of terrestrial and marine organic sources using biomarker parameters and partial least-squares (PLS) analysis. The PLS analysis can overcome the multicollinearity of independent variables and remove the disturbance caused by the multiple interpretations of biomarkers.[47] Multiple biomarker proxies are employed to eliminate the errors of individual biomarkers.

The screening of source proxies is a critical step. Parameters such as ACL, TAR, and P_{aq} from *n*-alkanes reveal the general composition of organic matter, while oleanane, bicadinanes, and taraxerane are specific to angiosperms.[35,41] The Pr/Ph ratio is controlled by both the organic matter source and the depositional environment.[26] $TT/C_{30}H$ can serve as an indicator of marine organic source input, since the tricyclic terpanes dominated by $C_{23}TT$ are related more with the algae source.[32] Owing to their linear correlation with TOC, the ACL, P_{aq}, TAR, Pr/Ph, and $TT/C_{30}H$ indicators can effectively characterize the relative intensity of terrestrial or marine organic material inputs (Figure 11a–d and f). It is noteworthy that there is a negative correlation between $TT/C_{30}H$ and TOC (Figure 11f), which seems to reflect the limiting effect of the algae input on organic matter enrichment. The detection of gammacerane suggests water stratification, where weak hydrodynamic conditions in a stratified water column are favorable for both algae growth and organic matter preservation in the Qiongdongnan Basin.[4] In the study area, most samples show low gammacerane/$C_{30}H$ values, with no apparent correlation observed with the TOC (Figure 11e). This may imply that the beneficial effect of slight water stratification on organic matter preservation counteracts the negative effect of increased algal productivity on organic matter enrichment. Despite the poor correlation between gammacerane/$C_{30}H$ and TOC, we propose that the abundance of gammacerane can still represent the contribution of marine organic material to a certain extent.

Oleanane, bicadinane T, and taraxerane are typical biomarkers derived from angiosperms.[35,40,41] The beautiful positive linear correlation between oleanane/$C_{30}H$ and taraxerane/$C_{30}H$ in Figure 12b suggests that they may share common biological precursors. The relative abundances of oleanane and bicadinanes were typically used to characterize the inputs of terrestrial organic materials in the past, theoretically showing a positive correlation with TOC. It is surprising that there is a very poor correlation between oleanane/$C_{30}H$ and TOC (Figure 11h) in the samples studied. As shown in Figure 12a, we observed two distinct trends between oleanane/$C_{30}H$ and $T/C_{30}H$. Samples from the delta front show higher and more variable oleanane/$C_{30}H$ but lower $T/C_{30}H$ (mostly below 1.0). Conversely, samples from the prodelta and inner shallow marine display relatively lower oleanane/$C_{30}H$ (typically below 0.5) but higher and wide-ranged $T/C_{30}H$ (up to 3.5).

Murray[48] proposed that contact with seawater may enhance the expression of oleananes in sediments during early diagenesis, but this perspective fails to fully explain the phenomenon where samples from the delta front (closer to the shore, with less contact with seawater) exhibit higher oleanane content. As a matter of fact, the spatial differences in the unload zone of terrigenous organic materials should be responsible for the interesting distributions of oleanane and bicadinanes in Figure 12a. The unloading of terrestrial organic materials in the delta-marginal sea system is a continuous process, with the delta front, prodelta, and inner shallow marine all being important depositional zones.[12,49] *β*-Amyrin, the precursor of oleanane, can be found in all plant sections but is enriched in the lignin of roots[50] and will convert into vitrinite during diagenesis. On the other hand, bicadinane is mainly derived from the resin of the *Dipterocarpaceae* (tropical rainforest species of Southeast Asia)[40] and will transform into exinite. The kerogen macerals in sediments are strongly influenced by the sedimentary facies in the delta-marginal sea system; shales deposited near the ocean typically show a higher exinite, while those closer to the land tend to contain higher vitrinite.[51] Therefore, the biological precursors of oleanane (woody debris) are more likely to be deposited in the delta front, while those of bicadinanes (resinous

https://doi.org/10.1021/acsomega.4c01777
ACS Omega 2024, 9, 22903−22922

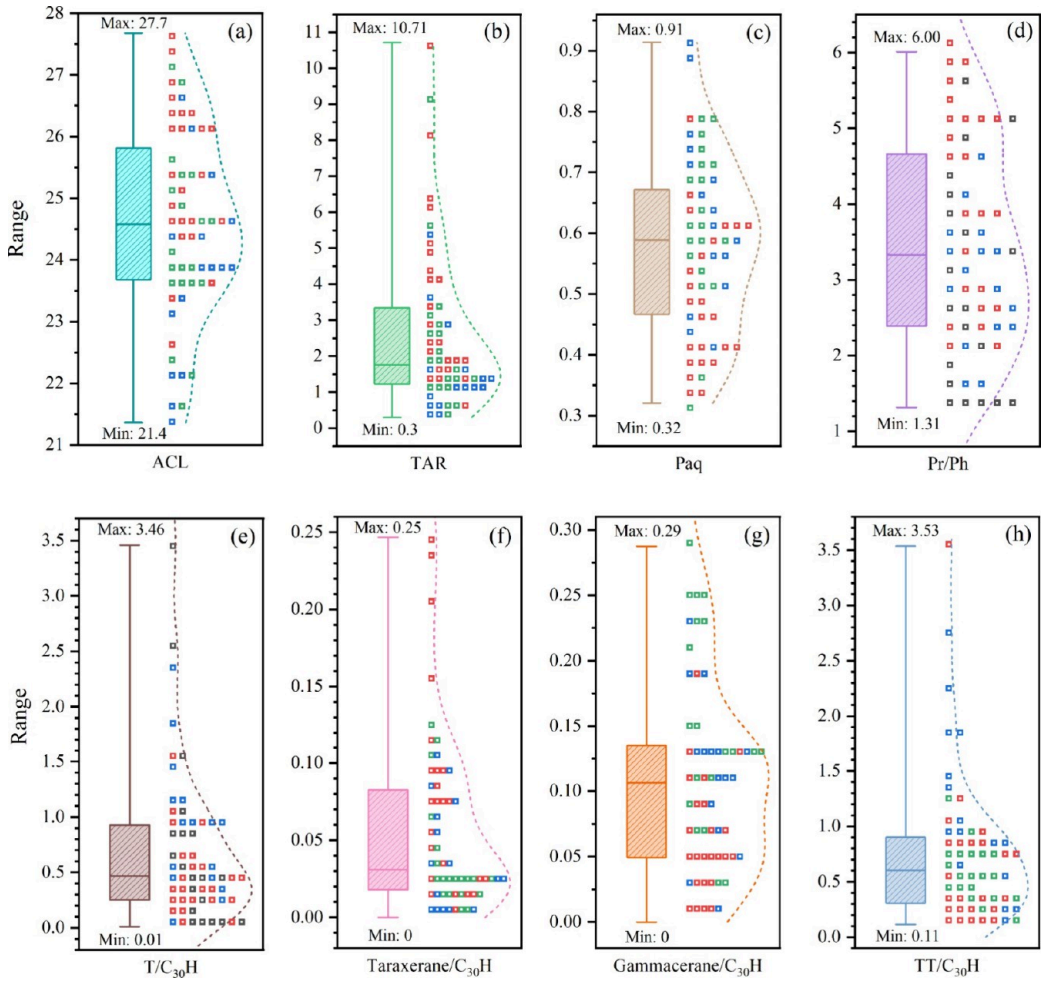

Figure 13. Distribution characteristics of source biomarker parameters (a) ACL, (b) TAR, (c) P_{aq}, (d) Pr/Ph, (e) T/C_{30}H, (f) taraxerane/C_{30}H, (g) gammacerane/C_{30}H, and (h) TT/C_{30}H (h). The definitions of these biomarker parameters are given in the footnote of Table 2.

debris) are prone to be buried in the prodelta and inner shallow marine. We suggest that the relationship between oleanane and bicadinane may serve as a potential sedimentological indicator of tertiary terrestrial organic materials in the delta-marginal marine system of Southeast Asia.

The differential unloading of terrestrial higher plant debris during the migration enhances the oleanane/C_{30}H in shales from the delta front, while the contact with seawater increases the oleanane/C_{30}H in these samples from the prodelta and inner shallow marine. It is worth mentioning that oleanane/C_{30}H is not a suitable proxy to reflect the input of terrestrial organic materials. The collective effect of seawater and differential unloading of terrestrial organic materials weakens the correlation between the oleanane content and TOC.

Although there is a good correlation between oleanane/C_{30}H and taraxerane/C_{30}H (Figure 12b), the synthetic pathways of oleanane (derives from β-amyrin) and taraxerane (originates from taraxerol, a component of cutinite) are quite different during the diagenesis.[38,41] The positive correlation between taraxerane/C_{30}H and TOC (Figure 11i) implies that the taraxerol appears independent of sedimentary facies and seawater during migration and diagenesis and can be regarded as an efficient source parameter. While the correlation between T/C_{30}H and TOC is poor for all studied shale samples, there is a certain positive correlation in the shales from the prodelta and inner shallow marine (Figure 11g). We believe that the content of bicadinanes still remains a reliable indicator of terrigenous organic matter.

Finally, we consider ACL, TAR, P_{aq}, Pr/Ph, TT/C_{30}H, gammcerane/C_{30}H, taraxerane/C_{30}H, and T/C_{30}H as efficient parameters for calculating the proportion of terrigenous and marine organic matter. Because of the similar maturation levels (low to moderate maturity) reflected by VR_r%, CPI, hopanoid and steroid parameters, the influence of thermal degradation on the biomarker parameters can be ignored for these shale samples.

5.3. Quantitative Assessment of Terrestrial Organic Matter in the Marine Source Rocks. On account of the great challenge of obtaining pure marine or terrestrial organic matter shale as endmember samples, we primarily determine the endmember values based on the distribution range of eight source biomarker parameters in all shale samples. The endmember values are set to be slightly greater than the maximum value and less than the minimum value of each parameter. Any one of the eight parameters should fall within the ranges between the corresponding parameters of pure marine and terrestrial endmembers; otherwise, the calculation results will exceed 100% or be a negative value.

Figure 13 displays the distribution patterns of the eight source biomarker parameters. For the pure terrestrial organic material endmember, we determine ACL as 28, TAR as 11, P_{aq} as 0.3, Pr/Ph as 6.0, T/C_{30}H as 3.5, taraxerane/C_{30}H as 0.25,

https://doi.org/10.1021/acsomega.4c01777
ACS Omega 2024, 9, 22903−22922

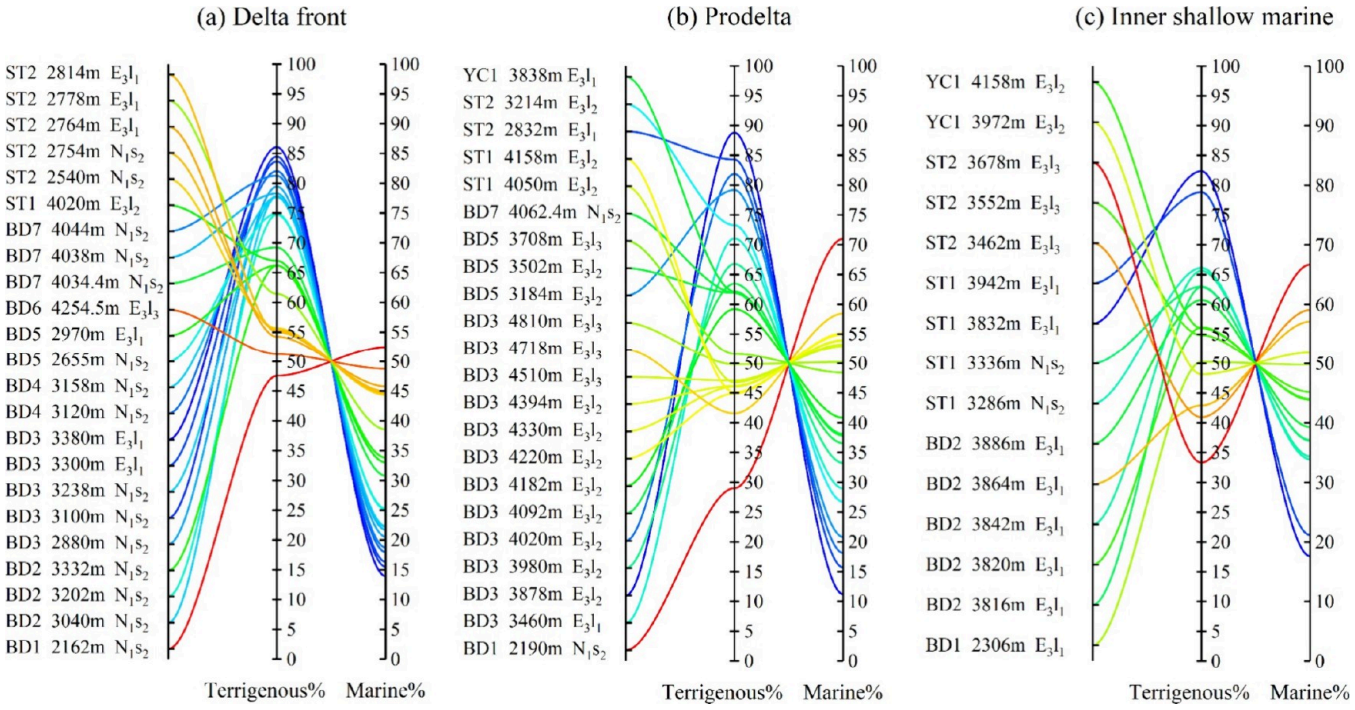

Figure 14. Parallel coordinate plots of relative proportions of terrigenous and marine organic matter in samples from the (a) delta front, (b) prodelta, and (c) inner shallow marine. The labels of these shale samples are composed of well name, sample depth, and stratigraphic unit.

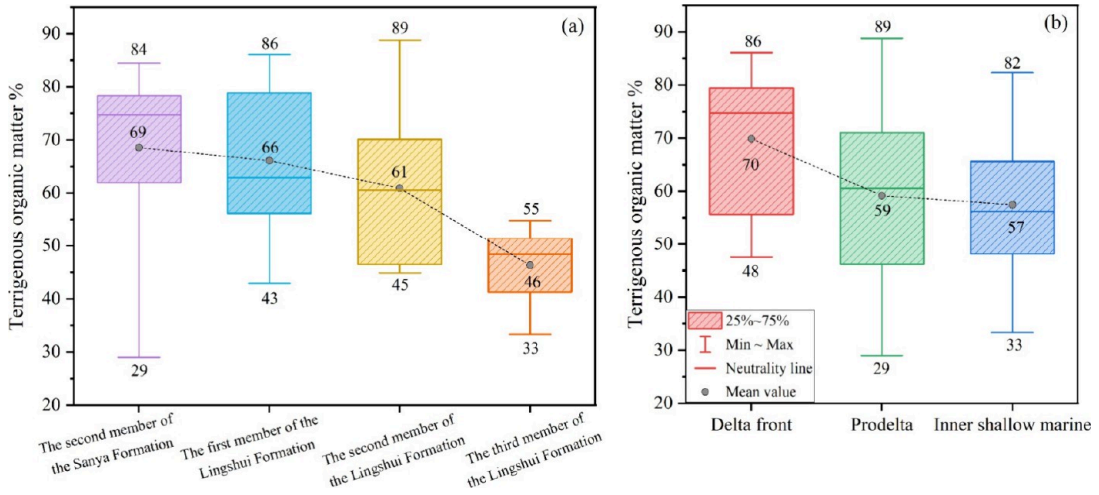

Figure 15. Distribution characteristics of terrestrial organic matter proportions based on (a) different target members and (b) different sedimentary facies.

gammacerane/C_{30}H as 0, and TT/C_{30}H as 0.11. On the contrary, the endmember values for pure marine organic source are established as follows: ACL as 21, TAR as 0.3, P_{aq} as 0.95, Pr/Ph as 1, T/C_{30}H as 0, taraxerane/C_{30}H as 0, gammacerane/C_{30}H as 0.3, and TT/C_{30}H as 3.6.

PLS analysis was conducted using OriginPro (Learning Edition). In the calculation process, virtual samples of pure terrestrial and marine organic sources were designated as independent variables, and the 60 shale samples collected in this research were set as dependent variables. The final calculation results for the total 60 shales are presented in the form of parallel coordinate plots based on sedimentary facies in Figure 14. There is a widely distributed range of terrigenous organic matter proportions in the studied shales, ranging from 29% to 89%, with an average of 63%. This finding supports the qualitative analysis viewpoint that terrigenous organic matter dominates the organic matter of the late Oligocene to early Miocene marine shales in the Qiongdongnan Basin.

The proportion of terrigenous organic matter gradually increases from the third member of the Lingshui Formation to the second member of the Sanya Formation (Figure 15a), consistent with the qualitative analysis results discussed above. Shales in the third member of Lingshui Formation have the lowest average terrigenous organic matter proportion at 46%. In comparison, samples from the second member of the Sanya Formation exhibit a wide range of terrigenous organic matter, varying from 29% to 84%, with the highest average being 69%.

Spatial differences in the unloading zone of oleanane and bicadinanes reveal the variations of terrigenous organic matter in different facies of the delta-marginal sea system (Figure 15b).

https://doi.org/10.1021/acsomega.4c01777
ACS Omega 2024, 9, 22903−22922

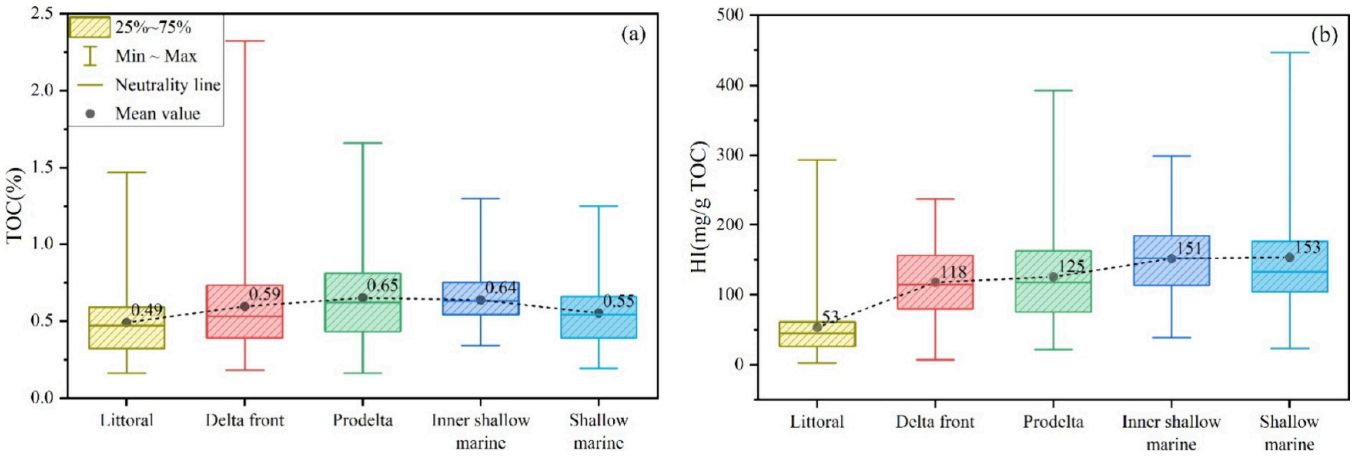

Figure 16. Distribution characteristics of (a) TOC and (b) HI based on different sedimentary facies from the coast toward the marine direction.

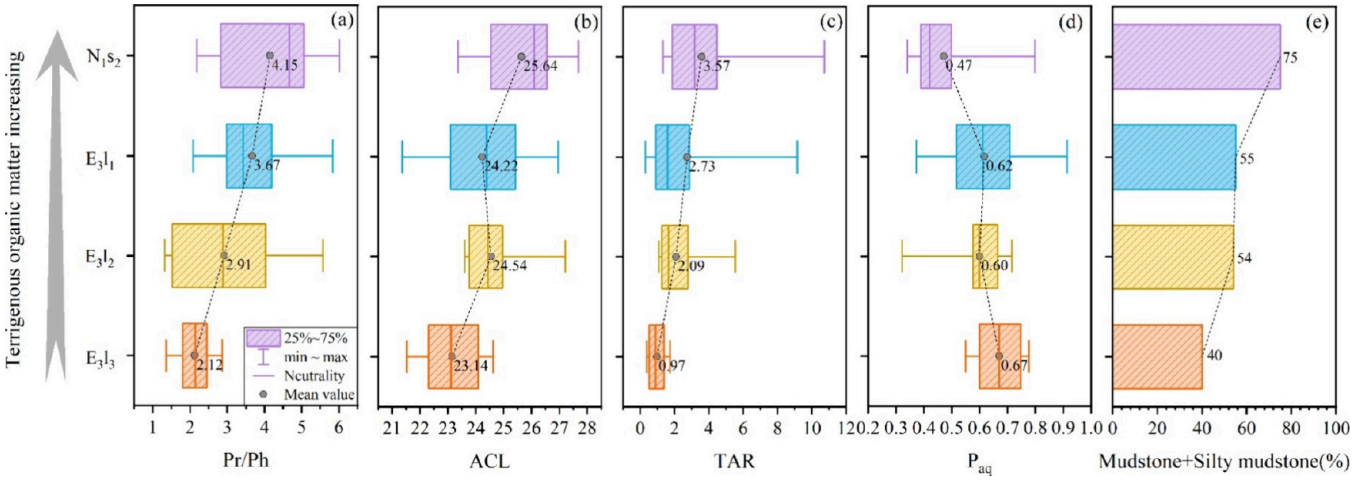

Figure 17. Distribution characteristics of Pr/Ph, ACL, TAR, Paq, and fine sediment proportions at different members. The meanings of stratigraphic unit abbreviations are shown in Figure 2.

The delta front appears to be the primary location for the unloading of terrigenous organic matter, with its highest proportion averaging 70%. This value progressively decreases in the prodelta and inner shallow marine, averaging 59% and 57%, respectively. It is well-known that shales dominated by terrestrial organic materials have a lower hydrocarbon index (HI), while those dominated by marine algae usually have a higher HI. The opposite trend between the terrestrial organic matter proportions (Figure 15b) and HI values (Figure 16b) across the delta front, prodelta, and inner shallow marine also confirms the credibility of our computational results. Moreover, the parallel proportions of terrigenous organic matter (range of 36−80%, average 63%) in the modern sediments of the Pearl River estuary,[15] as determined by carbon isotopic compositions, also enhance the confidence in our method. The differential unloading of terrestrial higher plant debris provides new insights into the mechanism and quantitative assessment of terrigenous organic matter accumulation in the delta-marginal sea system (Figure 18).

5.4. The Increase in Terrestrial Organic Materials Dominates the Organic Matter Accumulation. According to Table 1 and Figure 4, the TOC shows an increasing trend from the third member of the Lingshui Formation to the second member of the Sanya Formation. Organic carbon-rich shales are significantly controlled by bioproductivity and the preservation of biological precursors.[52] Biomarkers are effective tools in the study of the organic matter accumulation mechanism, since they provide a dual interpretation of environments and sources.[53,54] The positive correlations of TOC with ACL, TAR, Pr/Ph, T/C_{30}H, and taraxerane/C_{30}H (Figure 11a, c, d, g, and i), coupled with a negative correlation for P_{aq} (Figure 11b), suggest that the input of terrestrial higher plants plays a crucial role in the accumulation of organic carbon. Typically, a high Pr/Ph ratio in delta-marginal sea systems is associated more with the input of terrestrial organic materials under oxic conditions. The positive linear correlation of Pr/Ph with TOC (Figure 11d) further implies that the consumption of organic matter under oxic to suboxic conditions is covered by the substantial input of terrestrial organic materials in the Qiongdongnan Basin.

In contrast, there is a negative linear correlation between the TT/C_{30}H and TOC (Figure 11b and f), which can be explained as the low marine productivity being unable to compensate for the loss of organic matter under oxidative conditions. Evidence can be found in numerous HI and TOC data. From the coast toward the marine direction, the HI of shales gradually increases (Figure 16b), but relatively higher TOC values appear in three main depositional zones of terrestrial organic materials: delta front, prodelta area, and inner shallow marine (Figure 16 a). Although the delta front has the highest proportion of terrigenous organic matter, shales from the prodelta and the

https://doi.org/10.1021/acsomega.4c01777
ACS Omega 2024, 9, 22903−22922

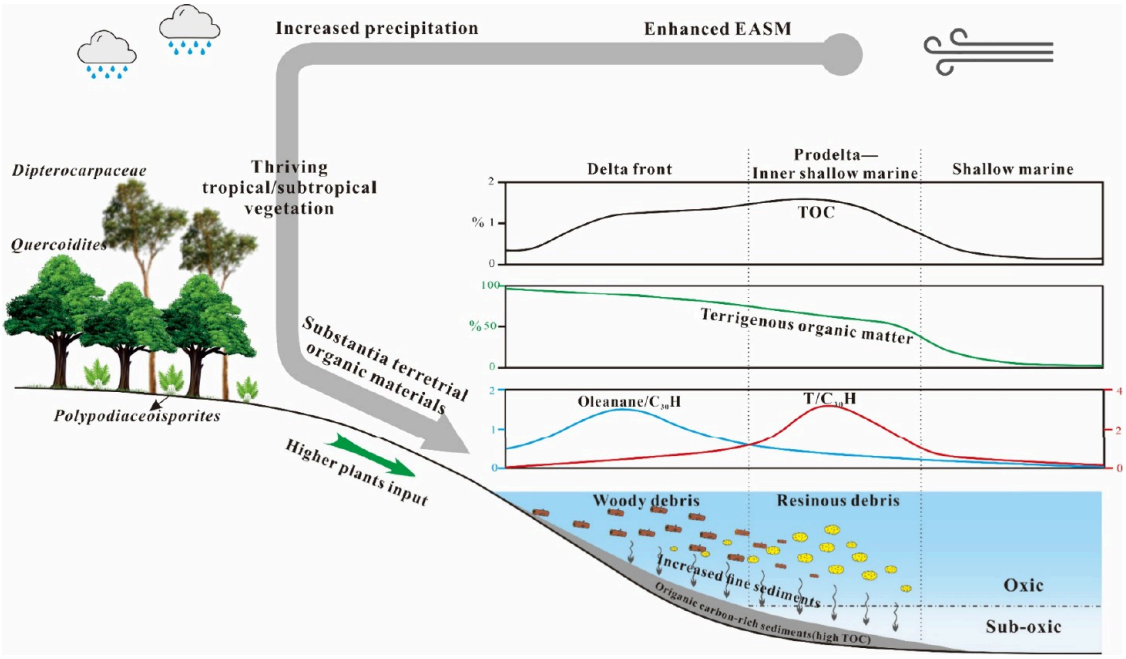

Figure 18. Schematic diagram illustrating the accumulation mechanism and quantitative assessment of terrigenous organic matter in the Qiongdongnan Basin. The typical vegetation taxa are determined based on the sporopollen and biomarkers characteristics. The variation curves of TOC and terrigenous organic matter proportion refer to the data presented in Figure 16a and Figure 15b, respectively. The variation curves of oleanane/C_{30}H and T/C_{30}H are based on the data shown in Figure 12a.

inner shallow marine exhibit the higher average TOC. The same signature has also been reported in the Magallanes Basin.[49] As shown in Figure 11d, a higher Pr/Ph ratio (average 3.98) indicates oxic conditions in the delta front, whereas the prodelta and inner shallow marine show suboxic conditions with lower Pr/Ph ratios (2.87 and 2.78, respectively). Similarly, higher gammacerane/C_{30}H (Figure 11e) suggests that the higher extent of water stratification in the prodelta and inner shallow marine is more favorable for the preservation of terrigenous organic matter.

In a word, an increased contribution of algae is not conducive to the enrichment of organic carbon, but the redox conditions of the water column should account for the differences in TOC between the delta front and prodelta-inner shallow marine.

As shown in Figure 17, the input of higher terrestrial plants gradually increases from the third member of the Lingshui Formation to the second member of the Sanya Formation. The sporopollen composition in the second member of the Sanya Formation (Figure 6) is characterized by plenty of tropical/subtropical broad-leveled taxa and pteridophytes, suggesting a warm and humid climate from 23 to 18.3 Ma. This climate change is likely caused by the strengthening of the East Asian summer monsoon between 24.9 and 18.3 Ma.[5]

The prevalence of EASM enhanced seasonal precipitation and surface runoff, which can further promote the channel mobility and land plants supply.[55] On the other hand, the enhanced coastal currents provoked by a moonsoon reduce the degradation of plant debris and are beneficial for the organic matter preservation.[56] Recent research has revealed that the increasing input of terrestrial higher plants in the channels can enhance the retention of mud through baffling, stabilization, and flocculation, providing benefits for the incorporation of terrigenous organic matter into the sediments.[57]

Evidence from extensive lithological data supports the view that increased input of terrigenous organic matter plays an important role in promoting the fine sediment content and organic matter abundance, as the mudstone proportion of sediments increases from the third member of the Lingshui Formation to the second member of the Sanya Formation (Table 1 and Figure 17e).

Based on the above discussions, we believe that the accumulation of organic matter in the Qiongdongnan Basin during the late Oligocene to early Miocene is mainly controlled by the intensity of the input of terrigenous organic materials driven by the EASM and warm climate rather than the bioproductivity of marine algae and preservation conditions of the water column (Figure 18). The warm climate and increased precipitation first benefit encourage the tropical-subtropical vegetation to flourish. The prevalence of EASM also enhanced the supply of terrestrial organic materials and fine sediment content, and then reduced the degradation of organic matter during transport and burial in the delta-marginal sea systems. The more reduced sedimentary environments of the prodelta and the inner shallow marine environment resulted in a higher organic matter abundance compared to that in the delta front.

6. CONCLUSIONS

(1) Terrigenous organic matter plays a significant role in the sediments of the delta-marginal sea system during late Oligocene to early Miocene in the Qiongdongnan Basin, and its proportion gradually increases from the third member of the Lingshui Formation to the second member of the Sanya Formation.

(2) The abundance differences of angiosperm-derived oleanane and bicadinanes across various sedimentary facies indicate the differential unloading of terrestrial organic materials. Woody debris of higher plants may be more extensively buried in the delta front, while resinous debris may be more abundant in the prodelta and inner shallow marine. The relative abundance of oleanane may

https://doi.org/10.1021/acsomega.4c01777
ACS Omega 2024, 9, 22903−22922

not fully represent the input intensity of terrestrial organic materials.

(3) Eight source biomarker parameters, including ACL, P_{aq}, TAR, Pr/Ph, gammacerane/C_{30}H, TT/C_{30}H, taraxerane/C_{30}H, and T/C_{30}H, are screened and employed to establish a calculation method for the proportion of terrigenous organic matter in sediments through PLS analysis. It is found that terrestrial organic matter input is highest in the delta front at 70%, followed by the prodelta at 59% and the inner shallow marine at 57%. As for the vertical signature, the proportions of terrestrial organic matter in shales from the third member of the Lingshui Formation to the second member of the Sanya Formation were determined to be 46%, 61%, 66%, and 69%, respectively.

(4) Terrestrial organic material input dominants the accumulation of organic matter rather than the bioproductivity of marine algae. Moreover, the redox conditions of the water column control the TOC value of organic carbon-rich sediments. The prevalence of the East Asian monsoon enhances the warm and humid climate, helping the tropical/subtropical vegetation thrive. The increase in the terrestrial higher plants supply prolongs the retention time of mud in the water column, leading to a positive feedback on the deposition of fine sediments, which also benefits the preservation of organic carbon.

APPENDIX

Molecular structures of biomarkers mentioned above.

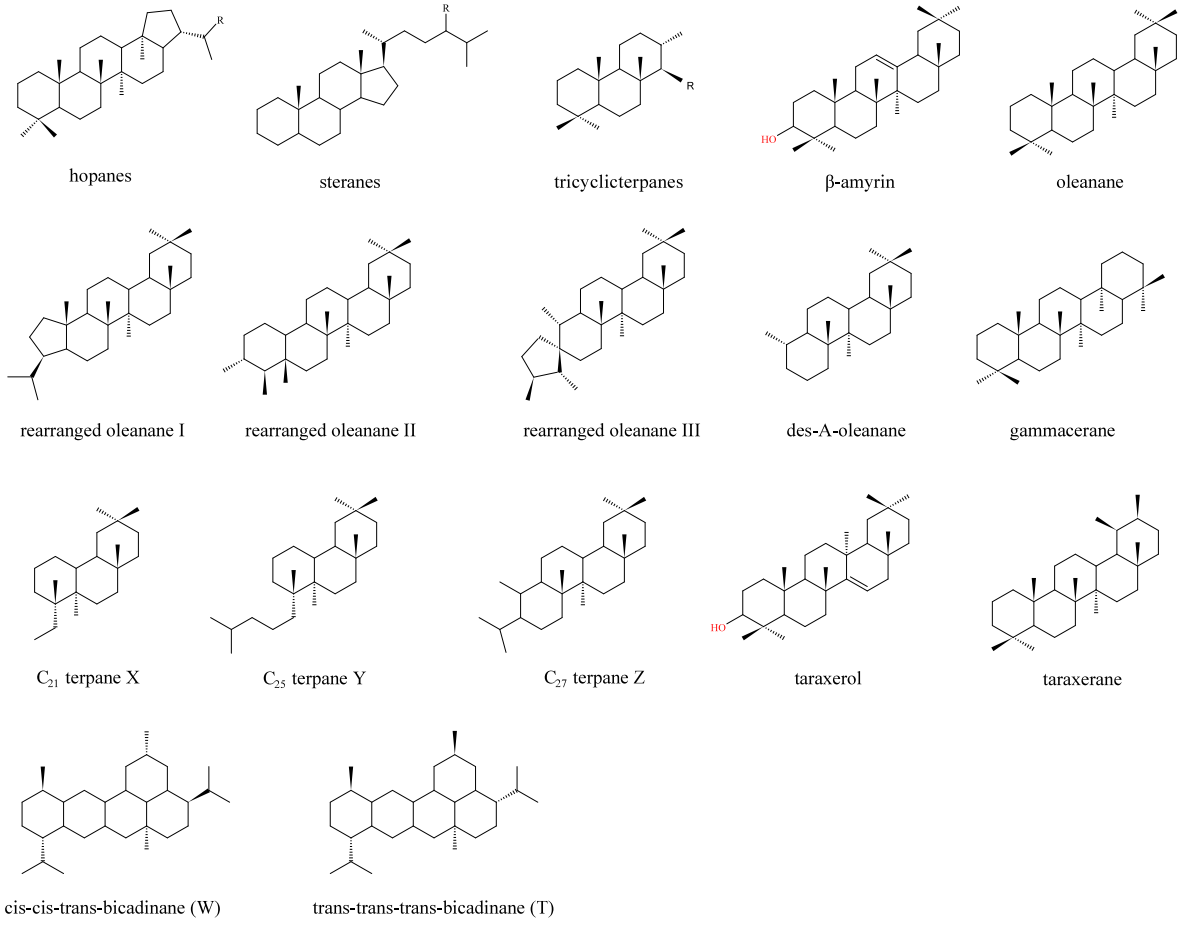

ASSOCIATED CONTENT

Supporting Information

The Supporting Information is available free of charge at https://pubs.acs.org/doi/10.1021/acsomega.4c01777.

Detailed TOC, rock pyrolysis, and vitrinite reflectance data (PDF)

AUTHOR INFORMATION

Corresponding Author

Dujie Hou − *School of Energy Resources, China University of Geosciences, Beijing 100083, China; Key Laboratory of Marine Reservoir Evolution and Hydrocarbon Accumulation Mechanism, Ministry of Education, Beijing 100083, China; Beijing Key Laboratory of Unconventional Natural Gas Geological Evaluation and Development Engineering, Beijing 100083, China;* orcid.org/0000-0003-2001-4082; Email: houdj313@163.com

Authors

Ziming Zhang − *School of Energy Resources, China University of Geosciences, Beijing 100083, China; Key Laboratory of Marine Reservoir Evolution and Hydrocarbon Accumulation Mechanism, Ministry of Education, Beijing 100083, China; Beijing Key Laboratory of Unconventional Natural Gas Geological Evaluation and Development Engineering, Beijing 100083, China;* orcid.org/0000-0002-1088-8256

Changgui Xu − *China National Offshore Oil Corporation, Beijing 100010, China*

Keqiang Wu − *China National Offshore Oil Corporation, Hainan, Haikou 570300, China*

https://doi.org/10.1021/acsomega.4c01777
ACS Omega 2024, 9, 22903−22922

Li You − *China National Offshore Oil Corporation, Hainan, Haikou 570300, China*
Xiong Cheng − *School of Energy Resources, China University of Geosciences, Beijing 100083, China; Key Laboratory of Marine Reservoir Evolution and Hydrocarbon Accumulation Mechanism, Ministry of Education, Beijing 100083, China; Beijing Key Laboratory of Unconventional Natural Gas Geological Evaluation and Development Engineering, Beijing 100083, China;* orcid.org/0000-0002-2991-1137
Xiaze Yan − *School of Energy Resources, China University of Geosciences, Beijing 100083, China; Key Laboratory of Marine Reservoir Evolution and Hydrocarbon Accumulation Mechanism, Ministry of Education, Beijing 100083, China; Beijing Key Laboratory of Unconventional Natural Gas Geological Evaluation and Development Engineering, Beijing 100083, China*
Weihe Chen − *School of Energy Resources, China University of Geosciences, Beijing 100083, China; Key Laboratory of Marine Reservoir Evolution and Hydrocarbon Accumulation Mechanism, Ministry of Education, Beijing 100083, China; Beijing Key Laboratory of Unconventional Natural Gas Geological Evaluation and Development Engineering, Beijing 100083, China*

Complete contact information is available at: https://pubs.acs.org/10.1021/acsomega.4c01777

Notes

The authors declare no competing financial interest.

■ ACKNOWLEDGMENTS

This project was funded by the National Natural Science Foundation of China (Grant 42302189).

■ REFERENCES

(1) Ding, W. J.; Hou, D. J.; Gan, J.; Wu, P.; Zhang, M. T.; George, S. C. Palaeovegetation variation in response to the late Oligocene-early Miocene East Asian summer monsoon in the Ying-Qiong Basin, South China Sea. *Palaeogeogr., Palaeoclimatol., Palaeoecol.* **2021**, *567*, 110205.
(2) Li, W. H.; Zhang, Z. H. Paleoenvironment and its control of the formation of Oligocene marine source rocks in the deep-water area of the northern South China Sea. *Energy Fuels* **2017**, *31* (10), 10598−10611.
(3) Liu, K.; Cheng, P.; Fan, C. W.; Song, P.; Huang, Q. T. Evolutions of sedimentary facies and palaeoenvironment and their controls on the development of source rocks in continental margin basins: A case study from the Qiongdongnan Basin, South China Sea. *Petro. Sci.* **2023**, *20* (5), 2648−2663.
(4) Wu, P.; Hou, D. J.; Gan, J.; Li, X.; Ding, W. J.; Liang, G.; Wu, B. B. Paleoenvironment and controlling factors of Oligocene source rock in the eastern deep-water area of the Qiongdongnan Basin: Evidences from organic geochemistry and palynology. *Energy Fuels* **2018**, *32* (7), 7423−7437.
(5) Ding, W. J.; Li, Y. C.; Lei, L.; Li, L.; Yang, S. C.; Yang, Y. C.; Hou, D. J. Biomarkers reveal the terrigenous organic matter enrichment in the late Oligocene-early Miocene marine shales in the Ying-Qiong Basin, South China Sea. *Acta Oceanol. Sin.* **2023**, *42* (3), 31−53.
(6) van der Hoeven, I. C.; Verreussel, R. M. C. H.; Riboulleau, A.; Tribovillard, N.; van de Schootbrugge, B. Climate-controlled organic matter accumulation as recorded in the Upper Jurassic Argiles de Châtillon Formation, a shallow-marine counterpart of the Kimmeridge Clay Formation. *Geol. Mag.* **2023**, *160* (3), 579−600.
(7) Xu, M.; Hou, D. J.; Cheng, X.; Gan, J.; Xu, X. D.; Liang, G.; Ding, W. J. Aliphatic biomarker signatures of early Oligocene—early Miocene source rocks in the central Qiongdongnan Basin: Source analyses of organic matter. *Acta Oceanol. Sin.* **2023**, *42* (3), 1−18.
(8) Hutchison, C. S. Marginal basin evolution: the southern South China Sea. *Mar. Petrol. Geol.* **2004**, *21* (9), 1129−1148.
(9) Sun, X. S.; Fan, D. J.; Liu, M.; Liao, H. J.; Tian, Y. The fate of organic carbon burial in the river-dominated East China Sea: Evidence from sediment geochemical records of the last 70 years. *Org. Geochem.* **2020**, *143*, 103999.
(10) Bao, R.; van der Voort, T. S.; Zhao, M. X.; Guo, X. Y.; Montluçon, D. B.; McIntyre, C.; Eglinton, T. I. Influence of hydrodynamic processes on the fate of sedimentary organic matter on continental margins. *Global Biogeochem. Cycles* **2018**, *32* (9), 1420−1432.
(11) Yu, M.; Eglinton, T. I.; Haghipour, N.; Montluçon, D. B.; Wacker, L.; Hou, P.; Ding, Y.; Zhao, M. Contrasting fates of terrestrial organic carbon pools in marginal sea sediments. *Geochim. Cosmochim. Ac.* **2021**, *309*, 16−30.
(12) Burdige, D. J. Burial of terrestrial organic matter in marine sediments: A re-assessment. *Global Biogeochem. Cycles* **2005**, *19* (4), 1−7.
(13) Chevalier, M.; Davis, B. A. S.; Heiri, O.; Seppä, H.; Chase, B. M.; Gajewski, K.; Lacourse, T.; Telford, R. J.; Finsinger, W.; Guiot, J.; et al. Pollen-based climate reconstruction techniques for late Quaternary studies. *Earth-Sci. Rev.* **2020**, *210*, 103384.
(14) Douglas, P. M. J.; Stratigopoulos, E.; Park, S.; Keenan, B. Spatial differentiation of sediment organic matter isotopic composition and inferred sources in a temperate forest lake catchment. *Chem. Geol.* **2022**, *603*, 120887.
(15) Hou, P. F.; Yu, M.; Eglinton, T. I.; Haghipour, N.; Zhang, H. L.; Zhao, M. X. Contrasting sources and fates of sedimentary organic carbon in subtropical estuary-marginal sea systems. *Chem. Geol.* **2023**, *638*, 121692.
(16) Imfeld, A.; Ouellet, A.; Douglas, P. M. J.; Kos, G.; Gélinas, Y. Molecular and stable isotope analysis ($\delta^{13}C$, $\delta^{2}H$) of sedimentary n-alkanes in the St. Lawrence Estuary and Gulf, Quebec, Canada: Importance of even numbered n-alkanes in coastal systems. *Org. Geochem.* **2022**, *164*, 104367.
(17) Lin, D. R.; Zhong, W.; Lin, Y. B.; Zhang, Y. D.; Li, T. H.; Quan, M. Y. Organic matter source traced by n-alkane records derived from lacustrine sediments from Daping swamp in the western Nanling Mountains (South China) and its response to climatic variability since the last deglacial. *Palaeogeogr., Palaeoclimatol., Palaeoecol.* **2022**, *605*, 111217.
(18) Huang, B. J.; Xiao, X. M.; Li, X. X. Geochemistry and origins of natural gases in the Yinggehai and Qiongdongnan basins, offshore South China Sea. *Org. Geochem.* **2003**, *34* (7), 1009−1025.
(19) Zhu, W. L.; Huang, B. J.; Mi, L. J.; Wilkins, R. W. T.; Fu, N.; Xiao, X. Geochemistry, origin, and deep-water exploration potential of natural gases in the Pearl River Mouth and Qiongdongnan basins, South China Sea. *AAPG Bull.* **2009**, *93* (6), 741−761.
(20) Tada, R.; Zheng, H. B.; Clift, P. D. Evolution and variability of the Asian monsoon and its potential linkage with uplift of the Himalaya and Tibetan Plateau. *Prog. Earth Planet. Sc.* **2016**, *3* (4), 1−26.
(21) Xie, X. N.; Müller, R. D.; Ren, J. Y.; Jiang, T.; Zhang, C. Stratigraphic architecture and evolution of the continental slope system in offshore Hainan, northern South China Sea. *Mar. Geol.* **2008**, *247* (3−4), 129−144.
(22) Eglinton, G.; Hamilton, R. J. Leaf epicuticular waxes. *Science* **1967**, *156*, 1322−1335.
(23) Cranwell, P. A. Lipids of Aquatic sediments and sedimenting particulates. *Prog. Lipid Res.* **1982**, *21*, 271−308.
(24) Ficken, K. J.; Li, B.; Swain, D. L.; Eglinton, G. An n-alkane proxy for the sedimentary input of submerged/floating freshwater aquatic macrophytes. *Org. Geochem.* **2000**, *31*, 745−749.
(25) Kennicutt, M. C.; Barker, C.; Brooks, J. M.; Defreitas, D. A.; Zhu, G. H. Selected organic-matter source indicators in the Orinoco, Nile and Changjiang Deltas. *Org. Geochem.* **1987**, *11* (1), 41−51.
(26) Peters, K. E.; Walters, C. C.; Moldowan, J. M. *The biomarker guide:Biomarkers and isotopes in petroleum exploration and earth history*; Cambridge University Press: Cambridge, UK, 2005.
(27) Nott, C. J.; Xie, S. C.; Avsejs, L. A.; Maddy, D.; Chambers, F. M.; Evershed, R. P. n-Alkane distributions in ombrotrophic mires as

indicators of vegetation change related to climatic variation. *Org. Geochem.* **2000**, *31* (2−3), 231−235.
(28) Meyers, P. A. Organic geochemical proxies of paleoceanographic, paleolimnologic, and paleoclimatic processes. *Org. Geochem.* **1997**, *27* (5−6), 213−250.
(29) Huang, W. Y.; Meinschein, W. G. Sterols as ecological indicators. *Geochim. Cosmochim. Ac.* **1979**, *43*, 739−745.
(30) Moldowan, J. M.; Seifert, W. K.; Gallegos, E. J. Relationship between petroleum composition and depositional environment of petroleum source rocks. *AAPG Bull.* **1985**, *69* (8), 1255−1268.
(31) Mackenzie, A. S.; Lamb, N. A.; Maxwell, J. R. Steroid hydrocarbons and the thermal history of sediments. *Nature.* **1982**, *295*, 223−226.
(32) Azevedo, D. A.; Neto, F. R. A.; Simoneit, B. R. T.; Pinto, A. C. Novel series of tricyclic aromatic terpanes characterized in Tasmanian tasmanite. *Org. Geochem.* **1992**, *18* (1), 9−16.
(33) Ourisson, G.; Albrecht, P.; Rohmer, M. The hopanoids: palaeochemistry and biochemistry of a group of natural products. *Pure. Appl. Chem.* **1979**, *51*, 709−729.
(34) Woodhouse, A. D.; Oung, J. N.; Philp, R. P.; Weston, R. J. Triterpanes and ring-a degraded triterpanes as biomarkers characteristic of Tertiary oils derived from predominantly higher-plant sources. *Org. Geochem.* **1992**, *18* (1), 23−31.
(35) Moldowan, J. M.; Dahl, J.; Huizinga, B. J.; Fago, F. J.; Hickey, L. J.; Peakman, T. M.; Taylor, D. W. The molecular fossil record of oleanane and its relation to angiosperms. *Science* **1994**, *265* (5173), 768−771.
(36) Nytoft, H. P.; Kildahl-Andersen, G.; Samuel, O. J. Rearranged oleananes: Structural identification and distribution in a worldwide set of Late Cretaceous/Tertiary oils. *Org. Geochem.* **2010**, *41* (10), 1104−1118.
(37) Samuel, O. J.; Kildahl-Andersen, G.; Nytoft, H. P.; Johansen, J. E.; Jones, M. Novel tricyclic and tetracyclic terpanes in Tertiary deltaic oils: Structural identification, origin and application to petroleum correlation. *Org. Geochem.* **2010**, *41* (12), 1326−1337.
(38) He, D.; Simoneit, B. R. T.; Cloutier, J. B.; Jaffé, R. Early diagenesis of triterpenoids derived from mangroves in a subtropical estuary. *Org. Geochem.* **2018**, *125*, 196−211.
(39) Lu, X. L.; Li, M. J.; Li, Y. C.; Yang, Y. C.; Wang, N.; Ran, Z. C.; Fu, Y.; Ali, S. Rearranged oleananes in Tertiary oils from the Baiyun Sag, Pearl River Mouth Basin, South China Sea: identification, distribution and geochemical significance. *Org. Geochem.* **2023**, *175*, 104525.
(40) van Aarssen, B. G. K.; Cox, H. C.; Hoogendoorn, P.; De Leeuw, J. W. A cadinene biopolymer in fossil and extant dammar resins as a source for cadinanes and bicadinanes in crude oils from South East Asia. *Geochim. Cosmochim. Ac.* **1990**, *54* (11), 3021−3031.
(41) Versteegh, G. J. M.; Schefuß, E.; Dupont, L.; Marret, F.; Sinninghe Damsté, J. S.; Jansen, J. H. F. Taraxerol and Rhizophora pollen as proxies for tracking past mangrove ecosystems. *Geochim. Cosmochim. Ac.* **2004**, *68* (3), 411−422.
(42) Sinninghe Damsté, J. S.; Kenig, F.; Koopmans, M. P.; Köster, J.; Schouten, S.; Hayes, J.M.; de Leeuw, J. W. Evidence for gammacerane as an indicator of water column stratification. *Geochim. Cosmochim. Ac.* **1995**, *59* (9), 1895−1900.
(43) Didyk, B. M.; Simoneit, B. R. T.; Brassell, S. C.; Eglinton, G. Organic geochemical indicators of palaeoenvironmental conditions of sedimentation. *Nature.* **1978**, *272*, 216−222.
(44) Shanmugam, G. Significance of coniferous rain forests and related organic matter in generating commercial quantities of oil, Gippsland Basin, Australia. *AAPG Bull.* **1985**, *69* (8), 1241−1254.
(45) Fathy, D.; Baniasad, A.; Littke, R.; Sami, M. Tracing the geochemical imprints of Maastrichtian black shales in southern Tethys, Egypt: Assessing hydrocarbon source potential and environmental signatures. *Int. J. Coal Geol.* **2024**, *283*, 104457.
(46) Summons, R. E.; Brassell, S. C.; Eglinton, G.; Evans, E.; Horodyski, R. J.; Robinson, N.; Ward, D. M. Distinctive hydrocarbon biomarkers from fossiliferous sediment of the Late Proterozoic Walcott Member, Chuar Group, Grand Canyon, Arizona. *Geochim. Cosmochim. Ac.* **1988**, *52*, 2625−2637.
(47) Wold, S.; Albano, C.; Dunn, W. J.; Esbensen, K.; Hellberg, S.; Johansson, E.; Lindberg, W.; Sjostrom, M. Modeling data tables by principal component and PLS: class patterns and quantitative predictive relations. *Analusis* **1984**, *12*, 477−485.
(48) Murray, A. P.; Sosrowidjojo, I. B.; Alexander, R.; Kagi, R. I.; Norgate, C. M.; Summons, R. E. Oleananes in oils and sediments: Evidence of marine influence during early diagenesis? *Geochim. Cosmochim. Ac.* **1997**, *61* (6), 1261−1276.
(49) Hage, S.; Romans, B. W.; Peploe, T. G. E.; Poyatos-Moré, M.; Ardakani, O. H.; Bell, D.; Englert, R. G.; Kaempfe-Droguett, S. A.; Nesbit, P. R.; Sherstan, G.; et al. High rates of organic carbon burial in submarine deltas maintained on geological timescales. *Nat. Geosci.* **2022**, *15* (11), 919−924.
(50) Otto, A.; Walther, H.; Puttmann, W. Molecular composition of a leaf-bearing and root-bearing Oligocene oxbow lake clay in the Weisselster Basin, Germany. *Org. Geochem.* **1994**, *22* (2), 275−286.
(51) Kang, H. Q.; Cheng, T.; Jia, H. C.; Bai, B.; Meng, J. L. The hydrocarbon generation characteristic of marine source rock in Meso-Cenozoic continental marginal basins. *Acta Pet. Sin.* **2017**, *38* (6), 649−657.
(52) Pedersen, T. F.; Calvert, S. E. Anoxia vs. productivity: what controls the formation of organic-carbon-rich sediments and sedimentary rocks? *AAPG Bull.* **1990**, *74* (4), 454−466.
(53) Summons, R. E.; Welander, P. V.; Gold, D. A. Lipid biomarkers: molecular tools for illuminating the history of microbial life. *Nat. Rev. Microbiol.* **2022**, *20* (3), 174−185.
(54) Abdelhady, A. A.; Seuss, B.; Jain, S.; Fathy, D.; Sami, M.; Ali, A.; Elsheikh, A.; Ahmed, M. S.; Elewa, A. M. T.; Hussain, A. M. Molecular technology in paleontology and paleobiology: Applications and limitations. *Quatern. Int.* **2024**, *685*, 24−38.
(55) Vimpere, L.; Spangenberg, J. E.; Roige, M.; Adatte, T.; De Kaenel, E.; Fildani, A.; Clark, J.; Sahoo, S.; Bowman, A.; Sternai, P.; et al. Carbon isotope and biostratigraphic evidence for an expanded Paleocene−Eocene Thermal Maximum sedimentary record in the deep Gulf of Mexico. *Geology* **2023**, *51* (4), 334−339.
(56) Liu, S.; Li, D. W.; Xiang, R.; Yu, M.; Zhang, H. L.; Li, L.; Zhao, M. X. Intensification of the East Asian winter monsoon resulted in greater preservation of terrestrial organic carbon on the inner shelf of the East China Sea since the last 1400 years. *Plaeogeogr., Palaeoclimatol., Palaeoecol.* **2023**, *615*, 111454.
(57) McMahon, W. J.; Davies, N. S.; Kleinhans, M. G.; Mitchell, R. L. Paleozoic vegetation increased fine sediment in fluvial and tidal channels: Evidence from secular changes to the mudrock content of ancient point bars. *Geology* **2023**, *51* (2), 136−140.

https://doi.org/10.1021/acsomega.4c01777
ACS Omega 2024, 9, 22903−22922